Appendix

Magnetostratigraphy across the end-Permian mass extinction event from the Meishan sections, southeastern China

Min Zhang[1,2,3], Hua-Feng Qin[2,4], Kuang He[1,2], Yi-Fei Hou[2,3,4], Quan-Feng Zheng[5], Cheng-Long Deng[2,3,4], Yan He[6], Shu-Zhong Shen[7,8*], Ri-Xiang Zhu[2,3,4], Yong-Xin Pan[1,2,3*]

[1]Chinese Academy Sciences (CAS) Key Laboratory of Earth and Planetary Physics, Institute of Geology and Geophysics, Chinese Academy of Sciences, Beijing 100029, China

[2]Innovation Academy for Earth Science, Chinese Academy of Sciences, Beijing 100029, China

[3]College of Earth and Planetary Sciences, University of the Chinese Academy of Sciences, Beijing 101400, China

[4]State Key Laboratory of Lithospheric Evolution, Institute of Geology and Geophysics, Chinese Academy of Sciences, Beijing 100029, China

[5]State Key Laboratory of Palaeobiology and Stratigraphy, Nanjing Institute of Geology and Palaeontology and Center for Excellence in Life and Paleoenvironment, Chinese Academy of Sciences, Nanjing 210008, China

[6]Agency of GSSP National Nature Reserve of Changxing, Zhejiang 313100, China

[7]State Key Laboratory for Mineral Deposits Research, School of Earth Sciences and Engineering and Environment and Frontiers Science Center for Critical Earth Material Cycling, Nanjing University, 163 Xianlin Avenue, Nanjing 210023, China

[8]Center for Excellence in Life and Paleoenvironment, Chinese Academy of Sciences, Nanjing 210023, China

* E-mails: yxpan@mail.iggcas.ac.cn, szshen@nju.edu.cn

A1: Geological Setting, Stratigraphy and Sampling

The Meishan sections (31°4.644′ N, 119°42.510′ E) are located at Changxing Country, Zhejiang Province, southeastern China. The base of Meishan sections are the uppermost part of late Permian Lungtan Formation, which is characterized by silty mudstone interbedded with thin-bedded calcareous sandstone and conformably overlain by the late Permian Changhsing Formation. The Changhsing Formation consists of dark grey bio-clastic packstone, greyish black thin-bedded carbonaceous and siliceous micrite, containing abundant fossils such as conodonts, ammonoids and fusulinids, which corresponds to the carbonate platform to offshore environmental system (Yin et al., 2001). The upper part of Meishan section is the early Triassic Yinkeng Formation overlaying on Changhsing Formation. The lower part of Yinkeng Formation is composed of grayish green calcareous mudstone intercalated by marl, and gray medium-thick bedded dolomitic micritic limestone, characterized by many cycles of mudstone-limestone and then developed into argillaceous limestone (Cao and Zheng, 2007; Sheng et al., 1984; Yin et al., 2001).

The Meishan sections have been divided into 60 beds, where the boundary between Lungtan Formation and Changhsing Formation is the lithological boundary of Bed 1 and 2 (Cao and Zheng, 2007; Chen et al., 2007). The end-Permian mass extinction (EPME) interval is constrained between Bed 25 and Bed 28 and Permian-Triassic boundary (PTB) was defined by the First Appearance Datum (FAD) of the conodont *Hindeodus parvus* in the middle of Bed 27. There are six sections in Changxing

Geological Relics National Nature Reserve, A, B, C, D, E and Z, among of them, section D has been ratified as the Global Stratotype Section and Point (GSSP) of PTB (Yin et al., 2001) and the base of Changhsingian Stage (Jin et al., 2006) by International Union of Geological Sciences (IUGS). In this study, we collected paleomagnetic samples from Meishan Sections C and D **(Fig. S1)**.

Total 305 samples were collected from the Section C from Bed 1 to Bed 41, and 344 samples were collected from the Section D from Bed 1 to Bed 29. The Yinkeng Formation at the Section D was covered by vegetation and inaccessible for sampling. In addition, and 11 paleomagnetic cores were drilled from a small fold in the bottom of Section C **(Fig. S5)** for a fold test. All samples were drilled using a portable gasoline-powered and water-cooled drill with non-magnetic diamond coring bits. An averaged sampling interval was 10 ~ 15 cm, and all samples were oriented *in situ* by using a magnetic compass, or both magnetic and sun compasses. For better description the results, we defined the boundary of Bed 1 and Bed 2 (the boundary between Lungtan Formation and Changhsing Formation) as 0 m for the apparent thickness (depth) in each section in this study.

A2: Rock magnetic measurements

Rock magnetic analyses were conducted to identify the magnetic carriers. The powder of fresh end material or parallel standard cylindrical specimens were prepared for isothermal remanent magnetization (IRM) acquisition curves and back-field

demagnetization curves, thermal demagnetization of three-component IRMs, and low-temperature measurements.

A2.1 IRM Acquisition Curves and its Back-field Demagnetization Curves

We measured IRM acquisition and its back-field curves on typical cylindrical specimens by utilizing 2G-760R cryogenic magnetometer and 2G 660 pulse magnetizer at room temperature. The specimens saturated rapidly below 200 mT and have the coercivities of remanence values (B_{cr}) less than ~100 mT **(Fig. S2-ii)**, indicative of soft magnetic carriers.

A2.3 Thermal Demagnetization of Three-component IRMs

Representative cylindrical specimens firstly were magnetized with 0.1 T, 0.3 T and 2.5 T along the X, Y and Z axes, respectively, by using a 2G Enterprises pulse magnetizer. These magnetized specimens were then subject to progressively thermal demagnetization up to 700 ℃ at 20 ℃ intervals for three orthogonal component IRMs (Lowrie, 1990), using a TDSC demagnetization oven, and remanence was measured with a 2G-760/755 cryogenic magnetometer. Results show that low-coercivity fractions is the dominant remanent magnetization carrier (**Fig. S2-iii**). A gradually decrease of remanence up to 550 ºC of low-coercivity component is probably carried by fine-grained magnetite.

A2.3 Low-temperature Measurements

Low-temperature measurements can identify magnetite with Verwey transition (Verwey, 1939), hematite with Morin transition (Morin, 1950) and / or pyrrhotite with

the Besnus transition (Rochette et al., 1990). In order to enhance the magnetic mineral concentration, magnetic extraction was conducted. Fresh end materials of samples were ground into powder by agate mortar, and then dissolved into a mildly acidic buffer solution (PH = 4) made of 2M CH_3COOH and 1M $NaCH_3COOH$ as 4:1 ratio (Strehlau et al., 2014) to dissolve calcite minerals. Temperature-dependence of saturation magnetization of the extractions were measured from 15 K to 300 K with applied field of 2.5 T, using Magnetic Property Measurement System-Extra Large 5 Superconducting Quantum Interference Device. The first - order derivatives of the curves show an obvious transition at ~125 K, confirming the existence of magnetite (**Fig. S2-iv**).

A4: Demagnetization of Natural Remanent Magnetization (NRM)

A4.1 Experimental Procedures

The paleomagnetic core samples were cut into standard-size cylindrical specimens (2.2 cm in length with 2.5 cm in diameter). All prepared specimens were subjected to stepwise thermal demagnetization using TD-PGL-100 thermal demagnetizer with an internal residual magnetic field less than 5 nT (Qin et al., 2020). Natural remanent magnetization (NRM) and subsequent remanent magnetizations after each demagnetization step for all specimens were measured by using 2G-RAPID cryogenic magnetometer with a sensitivity of $1*10^{-12}Am^2$ that is installed in magnetically shielded room (<300 nT). Each specimen was thermally demagnetized with 20°C interval until the maximum unblocking temperature was approached. These experiments were

conducted at the Paleomagnetism and Geochronology Laboratory (PGL), Institute of Geology and Geophysics, Chinese Academy of Sciences (IGGCAS) in Beijing, China.

A4.2 Paleomagnetic Results

In general, two components based on the demagnetization behaviors can be identified (**Fig. S3**). The low temperature component (LTC) is usually isolated from room temperature to 260 ℃. The direction cluster around the present dipole field (PDF) (D=354.2°, I=47.2°), which is a viscous remanence magnetization (**Fig. S4a**). The high temperature component (HTC) is isolated above 260 ℃ and decays toward to the origin of orthogonal vector plots. Total 435 specimens (67%) have the HTC component.

The paleomagnetic direction was calculated by principle component analysis (Kirschvink, 1980). The characteristic remanent magnetization (ChRM) direction was fit by at least 4 consecutive demagnetization steps of the HTC and 95% of maximum angular deviations (MAD) values are generally less than 15° (**Fig. S6**). Then the ChRMs were used to calculate the mean direction using Fisher statistics (Fisher, 1953). Notably, the mean normal directions and mean reversed direction of ChRM somewhat deviate from being antipodal with the normal one that have a steeper and better grouped tendency than the reverse (**Fig. S4**). This is probably due to less specimens of reversed direction and / or residual of overprinted remanence. Ten specimens from fold limbs obtained stable ChRM vector direction (**Table S2**). Eigen analysis implies that the 95% confident bounds (56 - 108%) include 100% (**Fig. S5**) (Tauxe and Watson, 1994), which suggests that fold test is positive.

Previous paleomagnetic studies have demonstrated that the South China Block (SCB) gradually drifted away from the equator to intermediate latitudes of the northern hemisphere with a clockwise rotation during the middle Permian to early Jurassic (Huang et al., 2018; Wu et al., 2017 and references therein). To minimize such effects, the specimen level VGPs were rotated to a coordinates system, where the mean P_3-T_1 paleomagnetic pole of SCB (Plon. / Plat. = 219.2º / 44.8º, A_{95} = 3.4º) (**Table S1**) was setting as the geographic pole using PmagPy software (Tauxe, 2010). The rotated VGP (rVGP) latitudes were then used to define the succession of magnetostratigraphic polarity (Kent et al., 2018). Both the VGP latitudes data before and after the coordinate system transferring were presented in **Fig. S7**.

REFERENCES CITED

Besse, J., Torcq, F., Gallet, Y., Ricou, L., Krystyn, L., and Saidi, A., 1998, Late Permian to Late Triassic palaeomagnetic data from Iran: constraints on the migration of the Iranian block through the Tethyan Ocean and initial destruction of Pangaea: Geophysical Journal International, v. 135, no. 1, p. 77-92.

Burov, B., 2005, Boundary between the Permian and Triassic rocks in the Moscow Syneclise reconstructed from the rock sequences exposed in the Kichmenga River basin: Russian Journal of Earth Sciences, v. 7, no. 2, p.107-114.

Cao, C., and Zheng, Q., 2007, High-resolution lithostratigraphy of the Changhsingian stage in Meishan section D, Zhejiang: Journal of Stratigraphy, v. 31, no. 1, p. 14-22.

Chen, Z. Q., Tong, J., Kaiho, K., and Kawahata, H., 2007, Onset of biotic and environmental recovery from the end-Permian mass extinction within 1-2 million years: A case study of the Lower Triassic of the Meishan section, South China: Palaeogeography Palaeoclimatology Palaeoecology, v. 252, no. 1-2, p. 176-187.

De Kock, M., and Kirschvink, J., 2004, Paleomagnetic constraints on the Permian-Triassic boundary in terrestrial strata of the Karoo Supergroup, South Africa: implications for causes of the end-Permian extinction event: Gondwana Research, v. 7, no. 1, p. 175-183.

Embleton, B. J., McElhinny, M. W., Ma, X., Zhang, Z., and Xiang Li, Z., 1996, Permo-Triassic magnetostratigraphy in China: the type section near Taiyuan, Shanxi province, North China: Geophysical Journal International, v. 126, no. 2, p. 382-388.

Enkin, R. J., Yang, Z. Y., Chen, Y., and Courtillot, V., 1992, Paleomagnetic constraints on the geodynamic history of the major blocks of china from the permian to the present: Journal of Geophysical Research: Solid Earth, v. 97, no. B10, p. 13953-13989.

Fisher, R., 1953, Dispersion on a sphere: Proceedings of the Royal Society of London Series a-Mathematical and Physical Sciences, v. 217, no. 1130, p. 295-305.

Gallet, Y., Krystyn, L., Besse, J., Saidi, A., and Ricou, L. E., 2000, New constraints on the Upper Permian and Lower Triassic geomagnetic polarity timescale from the Abadeh section (central Iran): Journal of Geophysical Research: Solid Earth, v. 105, no. B2, p. 2805-2815.

Gastaldo, R. A., Kamo, S. L., Neveling, J., Geissman, J. W., Bamford, M., and Looy, C. V., 2015, Is the vertebrate-defined Permian-Triassic boundary in the Karoo Basin, South Africa, the terrestrial expression of the end-Permian marine event?: Geology, v. 43, no. 10, p. 939-942.

Gastaldo, R. A., Neveling, J., Geissman, J. W., and Kamo, S. L., 2018, A lithostratigraphic and magnetostratigraphic framework in a geochronologic

context for a purported Permian-Triassic boundary section at Old (West) Lootsberg Pass, Karoo Basin, South Africa: Geological Society of America Bulletin, v. 130, no. 9-10, p. 1411-1438.

Gialanella, P., Heller, F., Haag, M., Nurgaliev, D., Borisov, A., Burov, B., Jasonov, P., Khasanov, D., Ibragimov, S., and Zharkov, I., 1997, Late Permian magnetostratigraphy on the eastern Russian platform: Geologie en Mijnbouw, v. 76, no. 1-2, p. 145-154.

Glen, J., Nomade, S., Lyons, J., Metcalfe, I., Mundil, R., and Renne, P., 2009, Magnetostratigraphic correlations of Permian–Triassic marine-to-terrestrial sections from China: Journal of Asian Earth Sciences, v. 36, no. 6, p. 521-540.

Gurevich, Y. L., and Slautsitays, I., 1985, A paleomagnetic section in the Upper Permian and Triassic deposits on Novaya Zemlya: International Geology Review, v. 27, no. 2, p. 168-177.

Gurevitch, E., Westphal, M., Daragan-Suchov, J., Feinberg, H., Pozzi, J., and Khramov, A., 1995, Paleomagnetism and magnetostratigraphy of the traps from Western Taimyr (northern Siberia) and the Permo-Triassic crisis: Earth and Planetary Science Letters, v. 136, no. 3-4, p. 461-473.

Gurevitch, E. L., Heunemann, C., Rad'ko, V., Westphal, M., Bachtadse, V., Pozzi, J. P., and Feinberg, H., 2004, Palaeomagnetism and magnetostratigraphy of the Permian–Triassic northwest central Siberian Trap Basalts: Tectonophysics, v. 379, no. 1-4, p. 211-226.

Haag, M., and Heller, F., 1991, Late Permian to early Triassic magnetostratigraphy: Earth and Planetary Science Letters, v. 107, no. 1, p. 42-54.

Haslett, J., and Parnell, A., 2008, A simple monotone process with application to radiocarbon‐dated depth chronologies: Journal of the Royal Statistical Society: Series C (Applied Statistics), v. 57, no. 4, p. 399-418.

Heller, F., Haihong, C., Dobson, J., and Haag, M., 1995, Permian-Triassic magnetostratigraphy—new results from South China: Physics of the Earth and Planetary Interiors, v. 89, no. 3-4, p. 281-295.

Heller, F., Lowrie, W., Huamei, L., and Junda, W., 1988, Magnetostratigraphy of the Permo-Triassic boundary section at Shangsi (Guangyuan, Sichuan Province, China): Earth and Planetary Science Letters, v. 88, no. 3, p. 348-356.

Huang, B., Yan, Y., Piper, J. D. A., Zhang, D., Yi, Z., Yu, S., and Zhou, T., 2018, Paleomagnetic constraints on the paleogeography of the East Asian blocks during Late Paleozoic and Early Mesozoic times: Earth-Science Reviews, v. 186, p. 8-36.

Iosifidi, A. G., and Khramov, A. N., 2009, Magnetostratigraphy of Upper Permian sediments in the southwestern slope of Pai-Khoi (Khei-Yaga River section): Evidence for the global Permian-Triassic crisis: Izvestiya, Physics of the Solid Earth, v. 45, no. 1, p. 3-13.

Jin, Y., Wang, Y., Henderson, C., Wardlaw, B. R., Shen, S., and Cao, C., 2006, The Global Boundary Stratotype Section and Point (GSSP) for the base of Changhsingian Stage (Upper Permian): Episodes, v. 29, no. 3, p. 175-182.

Kent, D. V., Olsen, P. E., Rasmussen, C., Lepre, C., Mundil, R., Irmis, R. B., Gehrels, G. E., Giesler, D., Geissman, J. W., and Parker, W. G., 2018, Empirical evidence for stability of the 405-kiloyear Jupiter-Venus eccentricity cycle over hundreds of millions of years: Proceedings of the National Academy of Sciences of the United States of America, v. 115, no. 24, p. 6153-6158.

Kirschvink, J., 1980, The least-squares line and plane and the analysis of palaeomagnetic data: Geophysical Journal International, v. 62, no. 3, p. 699-718.

Li, H., and Wang, J., 1989, Magnetostratigraphy of Permo-Triassic boundary section of Meishan of Changxing, Zhejiang: Science in China Series B-Chemistry, Life Sciences & Earth Sciences, v. 32, no. 11, p. 1401-1408.

Lowrie, W., 1990, Identification of ferromagnetic minerals in a rock by coercivity and unblocking temperature properties %J Geophysical Research Letters, v. 17, no. 2, p. 159-162.

Meng, X., Hu, C., Wang, W., and Liu, H., 2000, Magnetostratigraphic Study of Meishan Permian-Triassic Section, Changxing, Zhejiang Province, China: Journal of China University of Geosciences, no. 03, p. 167-171.

Morin, F. J., 1950, Magnetic susceptibility of alpha-Fe_2O_3 and alpha-Fe_2O_3 with added titanium: Physical Review, v. 78, no. 6, p. 819-820.

Nawrocki, J., 1997, Permian to Early Triassic magnetostratigraphy from the Central European Basin in Poland: Implications on regional and worldwide correlations: Earth and Planetary Science Letters, v. 152, no. 1-4, p. 37-58.

Nawrocki, J., 2004, The Permian–Triassic boundary in the Central European Basin: magnetostratigraphic constraints: Terra Nova, v. 16, no. 3, p. 139-145.

Parnell, A. C., Haslett, J., Allen, J. R. M., Buck, C. E., and Huntley, B., 2008, A flexible approach to assessing synchroneity of past events using Bayesian reconstructions of sedimentation history: Quaternary Science Reviews, v. 27, no. 19-20, p. 1872-1885.

Qin, H., Zhao, X., Liu, S., Paterson, G. A., Jiang, Z., Cai, S., Li, J., Liu, Q., and Zhu, R., 2020, An ultra-low magnetic field thermal demagnetizer for high-precision paleomagnetism: Earth, Planets and Space, v. 72, no. 1, p. 1-12.

Rochette, P., Fillion, G., Mattéi, J.-L., and Dekkers, M. J., 1990, Magnetic transition at 30–34 Kelvin in pyrrhotite: insight into a widespread occurrence of this mineral in rocks: Earth and Planetary Science Letters, v. 98, no. 3, p. 319-328.

Scholger, R., Mauritsch, H. J., and Brandner, R., 2000, Permian–Triassic boundary magnetostratigraphy from the southern Alps (Italy): Earth and Planetary Science Letters, v. 176, no. 3-4, p. 495-508.

Scholze, F., Wang, X., Kirscher, U., Kraft, J., Schneider, J. W., Götz, A. E., Joachimski, M. M., and Bachtadse, V., 2017, A multistratigraphic approach to

pinpoint the Permian-Triassic boundary in continental deposits: The Zechstein–Lower Buntsandstein transition in Germany: Global and Planetary Change, v. 152, p. 129-151.

Sheng, J.Z., Chen, C.Z., Wang, Y.G.., Rui, L., Liao, Z. T., Bando, Y., Ishii, K. I., Nakazawa, K., and Nakamura, K., 1984, Permian-Triassic boundary in middle and eastern Tethys: Journal of Faculty of Science of Hokkaido University, v. 21, no. 1, p. 133-181.

Steiner, M., Ogg, J., Zhang, Z., and Sun, S., 1989, The late Permian/early Triassic magnetic polarity time scale and plate motions of south China: Journal of Geophysical Research Solid Earth, v. 94, no. B6, p. 7343-7363.

Strehlau, J. H., Hegner, L. A., Strauss, B. E., Feinberg, J. M., and Penn, R. L., 2014, Simple and Efficient Separation of Magnetic Minerals From Speleothems and Other Carbonates: Journal of Sedimentary Research, v. 84, no. 11, p. 1096-1106.

Szurlies, M., 2007, Latest Permian to Middle Triassic cyclo-magnetostratigraphy from the Central European Basin, Germany: implications for the geomagnetic polarity timescale: Earth and Planetary Science Letters, v. 261, no. 3-4, p. 602-619.

Szurlies, M., Bachmann, G. H., Menning, M., Nowaczyk, N. R., and Käding, K. C., 2003, Magnetostratigraphy and high-resolution lithostratigraphy of the Permian–Triassic boundary interval in Central Germany: Earth and Planetary Science Letters, v. 212, no. 3-4, p. 263-278.

Szurlies, M., Geluk, M. C., Krijgsman, W., and Kürschner, W. M., 2012, The continental Permian–Triassic boundary in the Netherlands: Implications for the geomagnetic polarity time scale: Earth and Planetary Science Letters, v. 317, p. 165-176.

Tauxe, L., 2010, Essentials of paleomagnetism, University of California Press.

Tauxe, L., and Watson, G. S., 1994, The fold test - an eigen analysis approach: Earth and Planetary Science Letters, v. 122, no. 3-4, p. 331-341.

Verwey, E. J. W., 1939, Electronic conduction of magnetite (Fe_3O_4) and its transition point at low temperatures: Nature, v. 144, p. 327-328.

Ward, P. D., Botha, J., Buick, R., De Kock, M. O., Erwin, D. H., Garrison, G. H., Kirschvink, J. L., and Smith, R., 2005, Abrupt and gradual extinction among Late Permian land vertebrates in the Karoo Basin, South Africa: Science, v. 307, no. 5710, p. 709-714.

Wu, L., Kravchinsky, V. A., and Potter, D. K., 2017, Apparent polar wander paths of the major Chinese blocks since the Late Paleozoic: Toward restoring the amalgamation history of east Eurasia: Earth-Science Reviews, v. 171, p. 492-519.

Yin, H. F., Zhang, K. X., Tong, J. N., Yang, Z. Y., and Wu, S. B., 2001, The Global Stratotype Section and Point (GSSP) of the Permian-Triassic Boundary: Episodes, v. 24, no. 2, p. 102-114.

Zhu, Y., and Liu, Y., 1999, Magnetostratigraphy of the Permo-Triassic boundary section at Meishan, Changxing, Zhejiang province, in Proceedings Proceedings of the International Conference on Pangea and the Paleozoic–Mesozoic Transition. China University of Geosciences Press, Wuhan, p. 79-84.

Appendix Figures

Figure S1: Location and field outcrop pictures of Meishan sections.

Figure S2: Rock magnetic results

Figure S3. Thermal demagnetization diagrams in stratigraphic coordinates system.

Figure S4: Stereo plots of magnetic component directions.

Figure S5: Fold test.

Figure S6: The histogram of maximum angular deviations (MAD) values.

Figure S7: The VGP latitudes of the original results and rotated results, respectively.

Figure S8: The Bayesian age-depth model for the Meishan sections.

Appendix Tables

Table S1: Paleomagnetic pole from the South China Block

Table S2: Sampling information and ChRM directions of fold test.

Table S3: The ChRM directions of Meishan Section C.

Table S4: The ChRM directions of Meishan Section D.

Table S5: The previously published documents about magnetostratigraphy of PTB sections

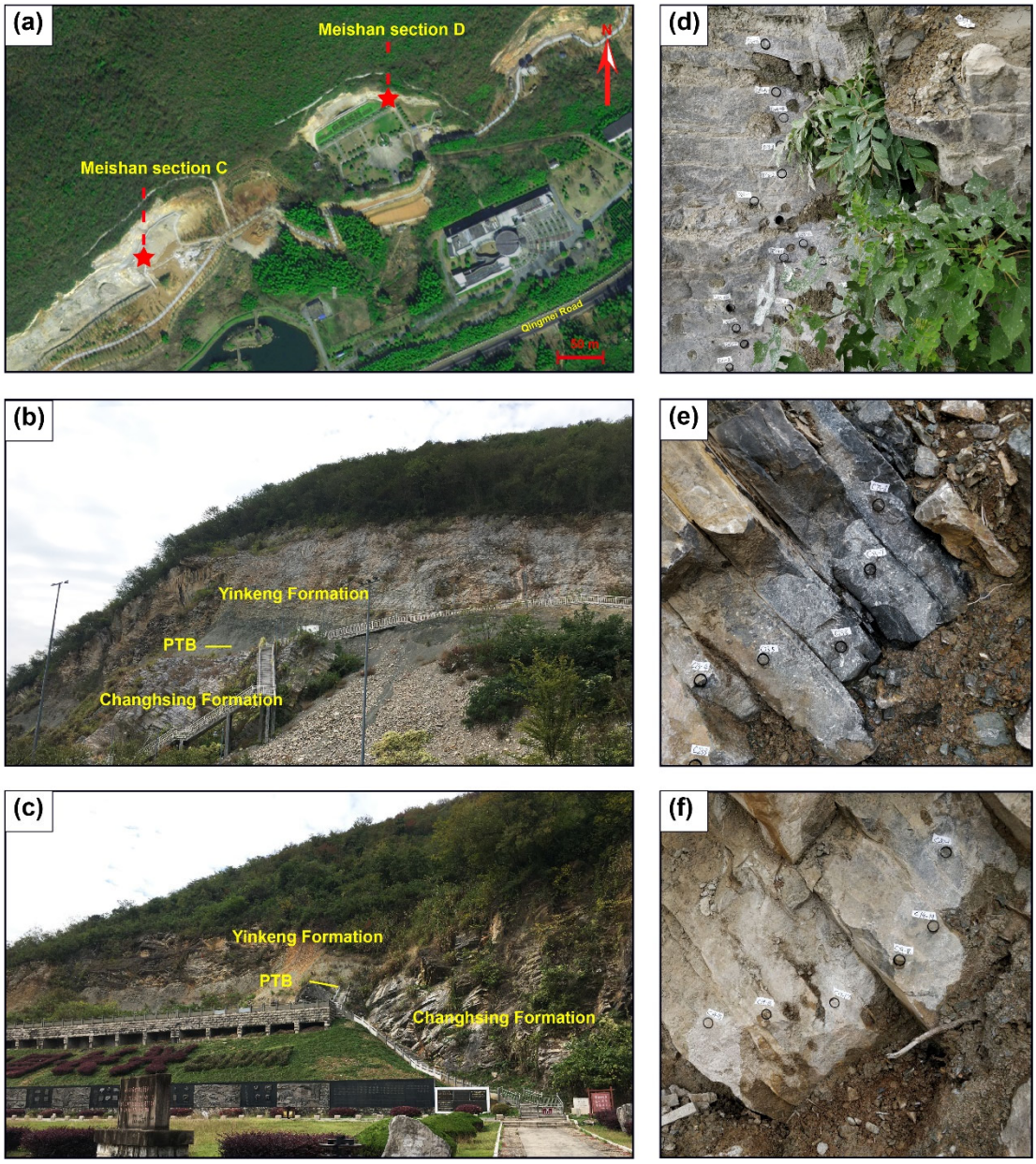

Figure S1. Outcrops of the Meishan section. (a) Location of Meishan section C and D. (b, c) Outcrop of Meishan section C and D, respectively. (d~f) field pictures of sampling. PTB, Permian-Triassic boundary.

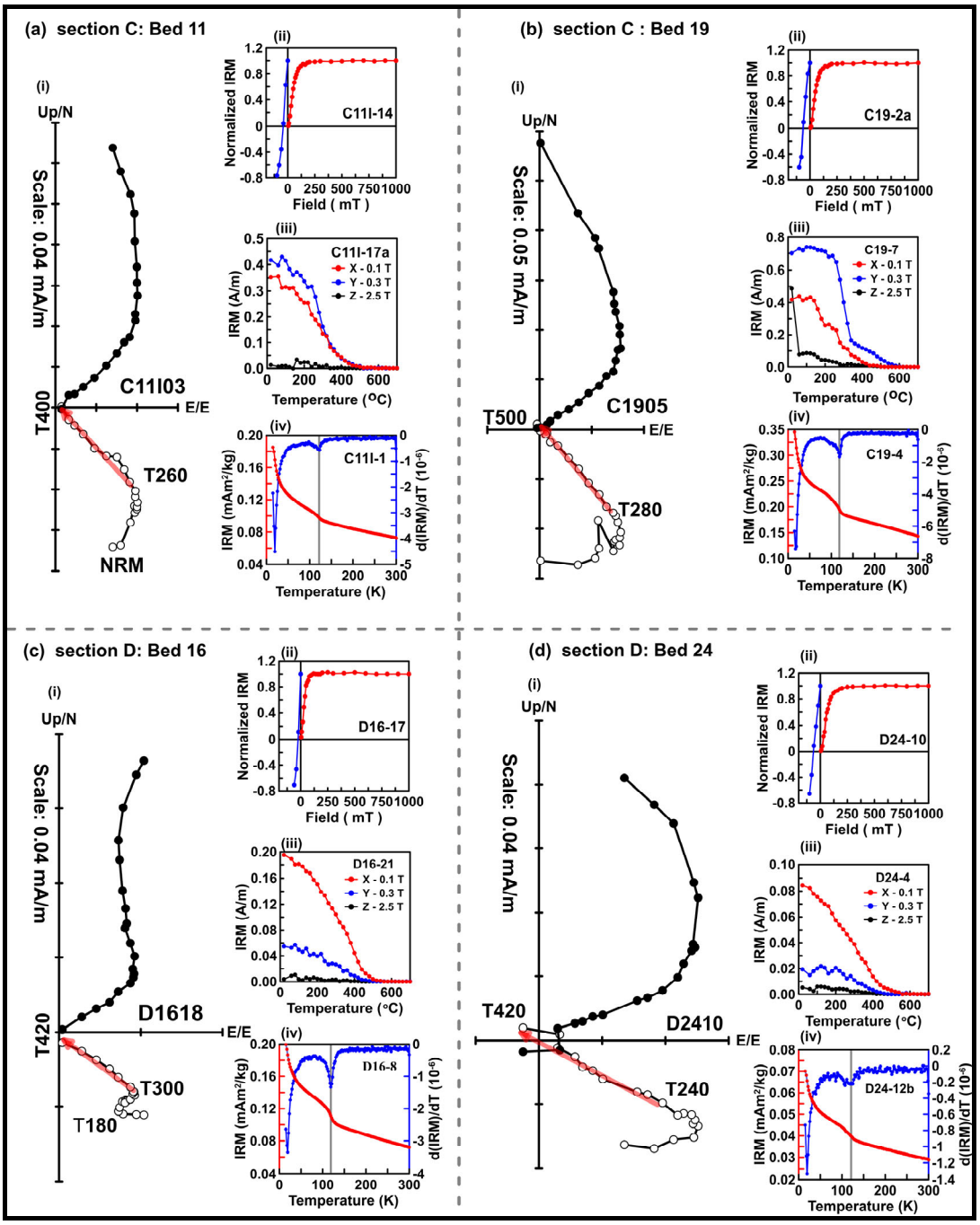

Figure S2. Rock magnetic results of the representive Beds. (i) Orthogonal plots of thermal demagnetization in stratigraphic coordinates. (ii) Isothermal remanent magnetization (IRM) acquisition curves and its back-field demagnetization curves for representative specimens. (iii) Stepwise thermal demagnetization of three orthogonal component IRMs.Each specimen was magnetized in 0.1 T, 0.3 T and 2.5 T field along X-, Y- and Z-axes, respectively. (iv) Low temperature demagnetization measurements (red dots and lines) of SIRM acquired at 300 K in a static field of 2.5 T and their corresponding first-order derivative curve (blue dots and lines) of representative specimens. The vertical gray line marks the Verwey transition temperature of magnetite.

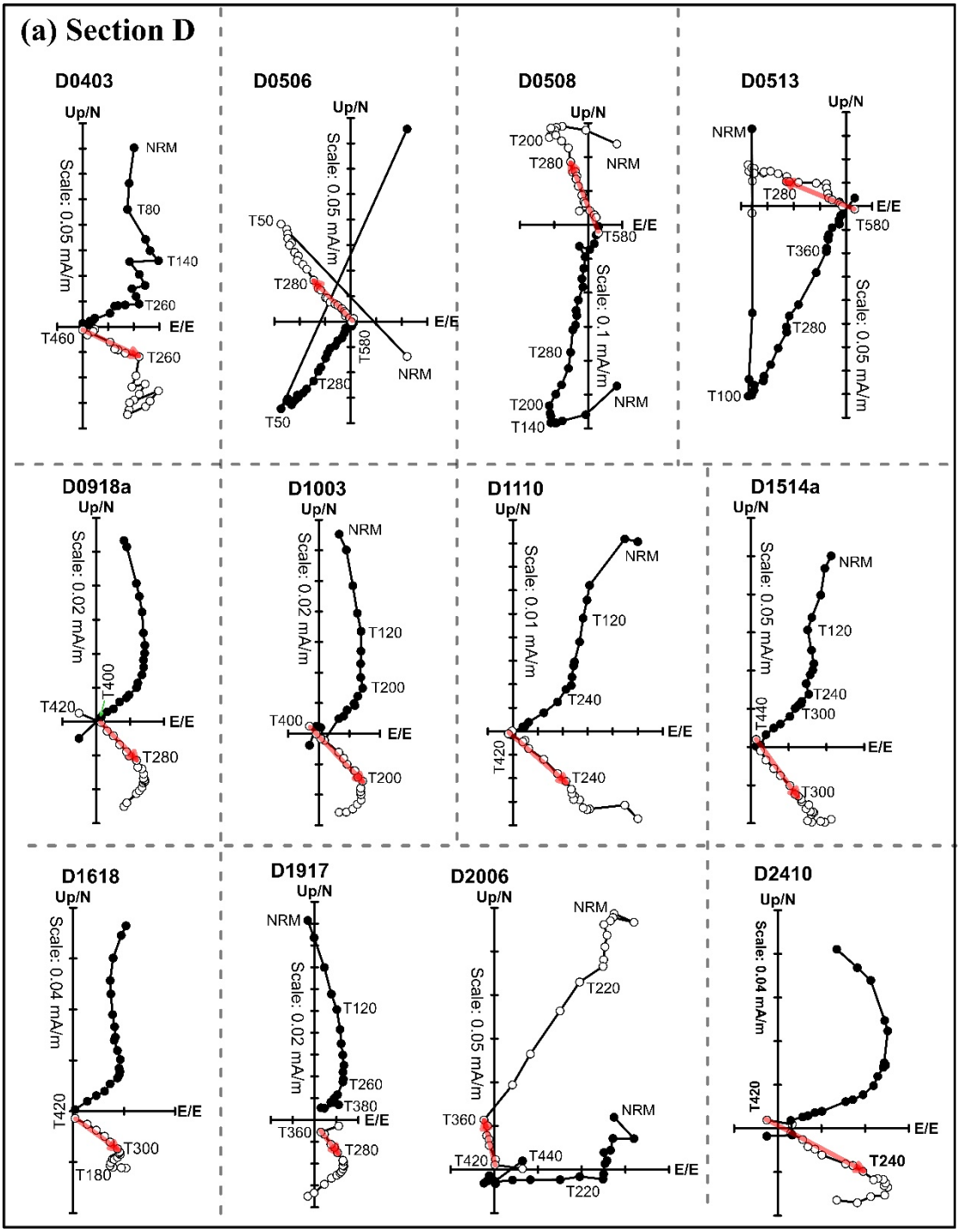
(a) Section D
D0403
Up/N
Scale: 0.05 mA/m
NRM
T80
T140
T260
E/E
T460
T260
D0506
Up/N
Scale: 0.05 mA/m
T50
T280
E/E
T580
NRM
T280
T50
D0508
Up/N
T200
T280
NRM
E/E
T580
Scale: 0.1 mA/m
T280
T200
T140
NRM
D0513
Up/N
NRM
T280
E/E
T580
T360
T280
T100
Scale: 0.05 mA/m
D0918a
Up/N
Scale: 0.02 mA/m
T400
T420
E/E
T280
D1003
Up/N
Scale: 0.02 mA/m
NRM
T120
T200
T400
E/E
T200
D1110
Up/N
Scale: 0.01 mA/m
NRM
T120
T240
E/E
T420
T240
D1514a
Up/N
Scale: 0.05 mA/m
NRM
T120
T240
T300
T440
E/E
T300
D1618
Up/N
Scale: 0.04 mA/m
T420
E/E
T300
T180
D1917
Up/N
NRM
Scale: 0.02 mA/m
T120
T260
T380
E/E
T360
T280
D2006
Up/N
NRM
T220
Scale: 0.05 mA/m
T360
NRM
T420
T440
E/E
T220
D2410
Up/N
Scale: 0.04 mA/m
T420
E/E
T240

(continued)

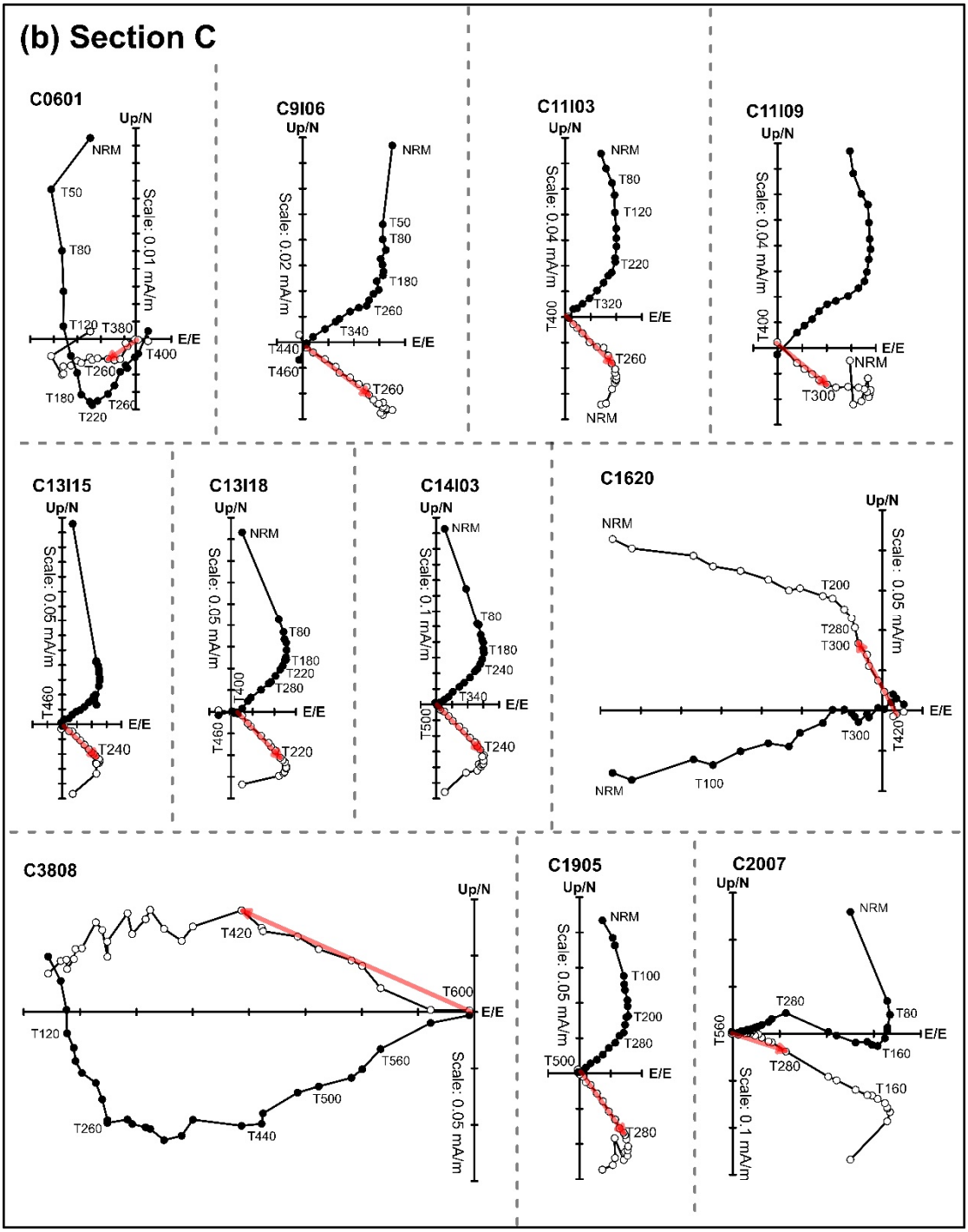

Figure S3. Orthogonal plots of thermal demagnetization of representative specimens in stratigraphic coordinates. (a) Meishan Section D; (b) Meishan Section C. Solid (open) circles denote horizontal (vertical) projection. Red arrows show the ChRM vector direction.

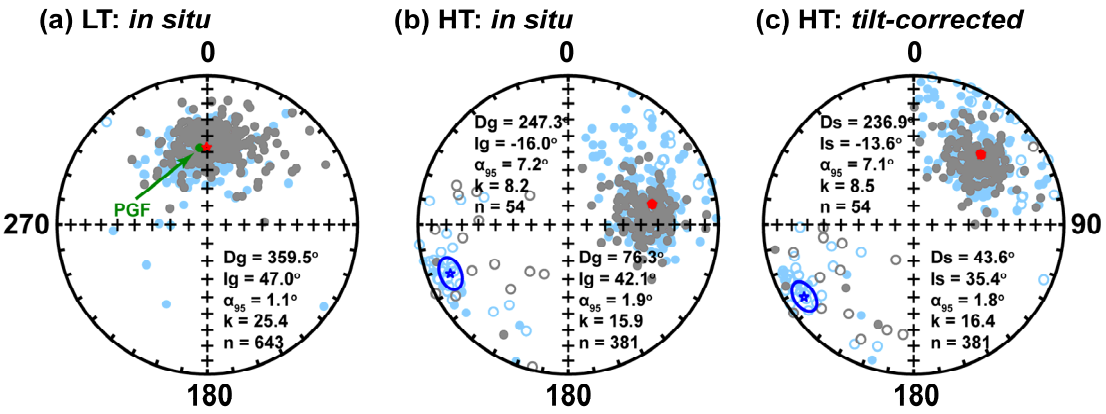

Figure S4. Stereo plots of magnetic component directions, light blue/grey circles denoted to the specimens of Meishan Sections C/D, respectively. (a) Low-temperature (LT) component in situ coordinates. PGF, the present geomagnetic field. High-temperature (HT) component in situ (b) and tilt-corrected (c) coordinates. Open (solid) circles designate projections of vectors on the upper (lower) hemisphere.

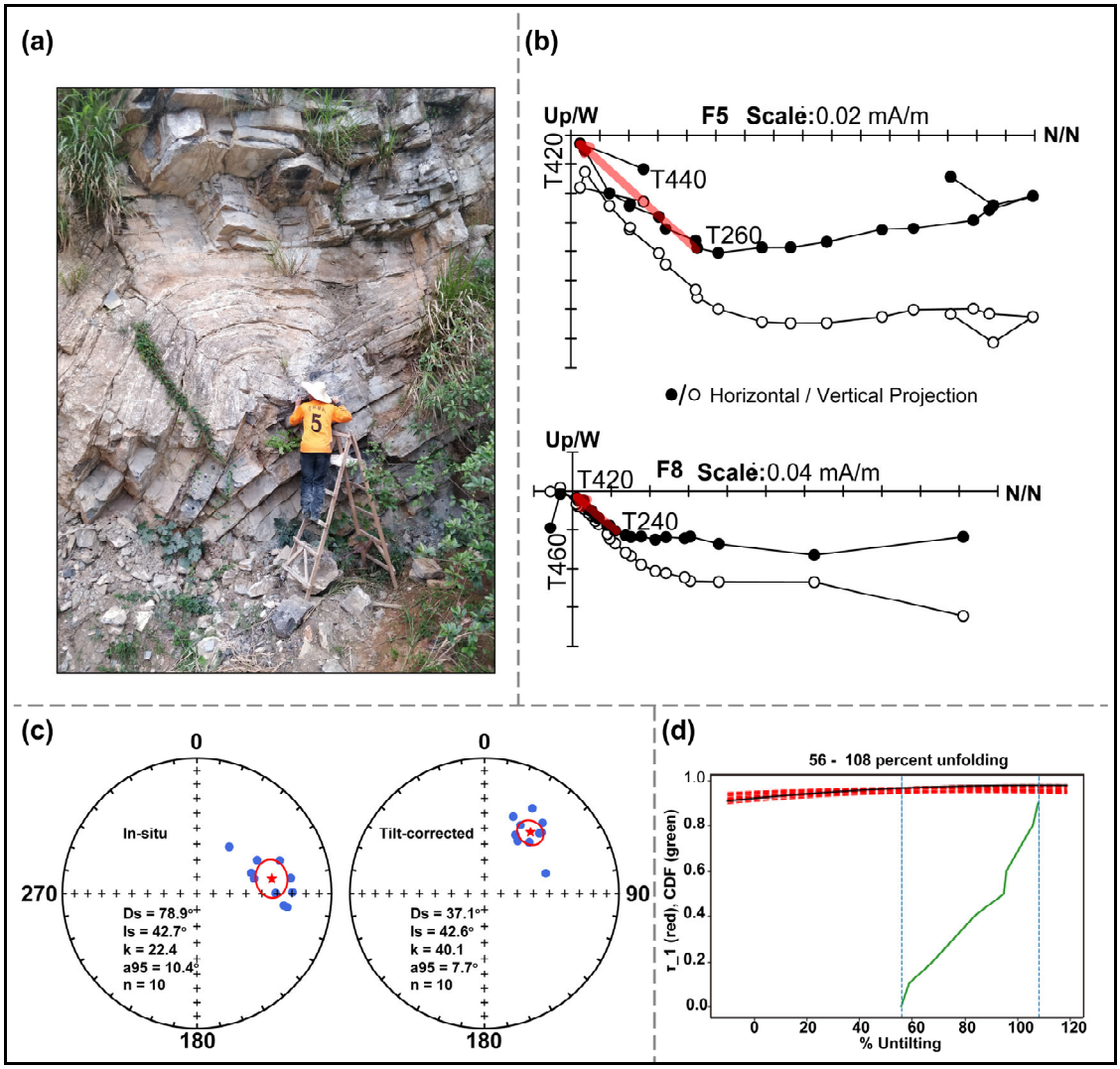

Figure S5. Fold test. (a) Photograph of the fold at the lower part of Meishan Section C. (b) Orthogonal projection diagrams of typical thermal demagnetization for fold specimens in stratigraphic coordinates. (c) Equal area projection of the high-temperature component directions of fold specimens before and after tilt corrections. (d) Eigen accumulation of unfolding analysis (Tauxe and Watson, 1994).

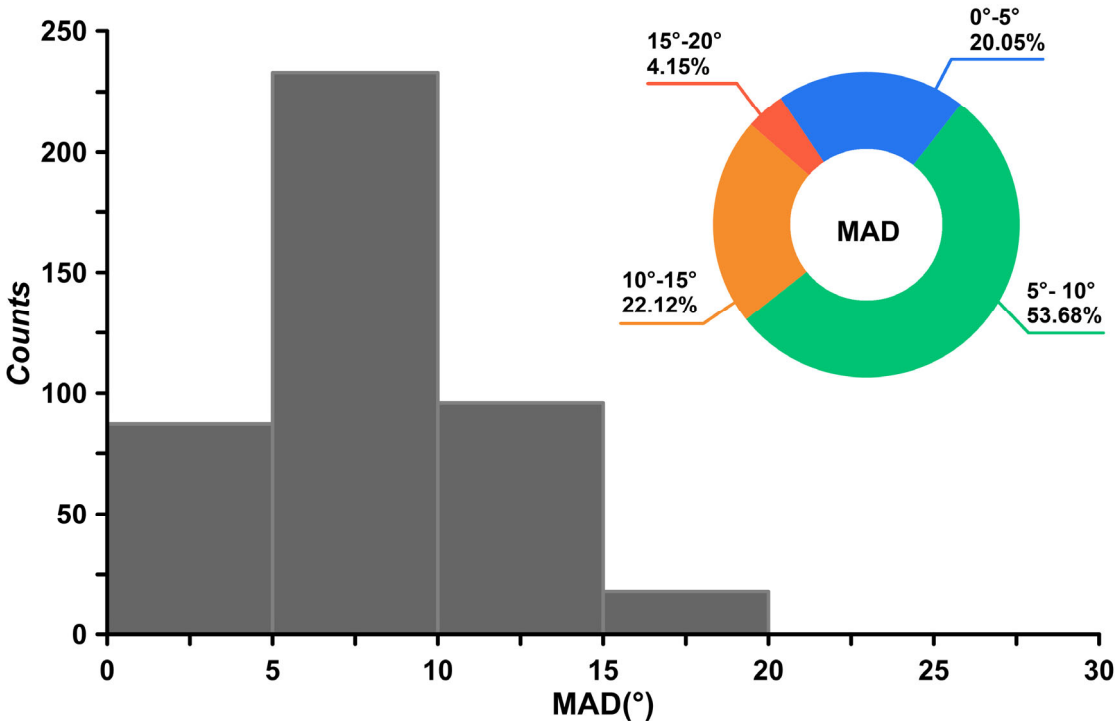

Figure S6. The histogram of maximum angular deviations (MAD). The inserted figure shows the percentage of each grouped MAD.

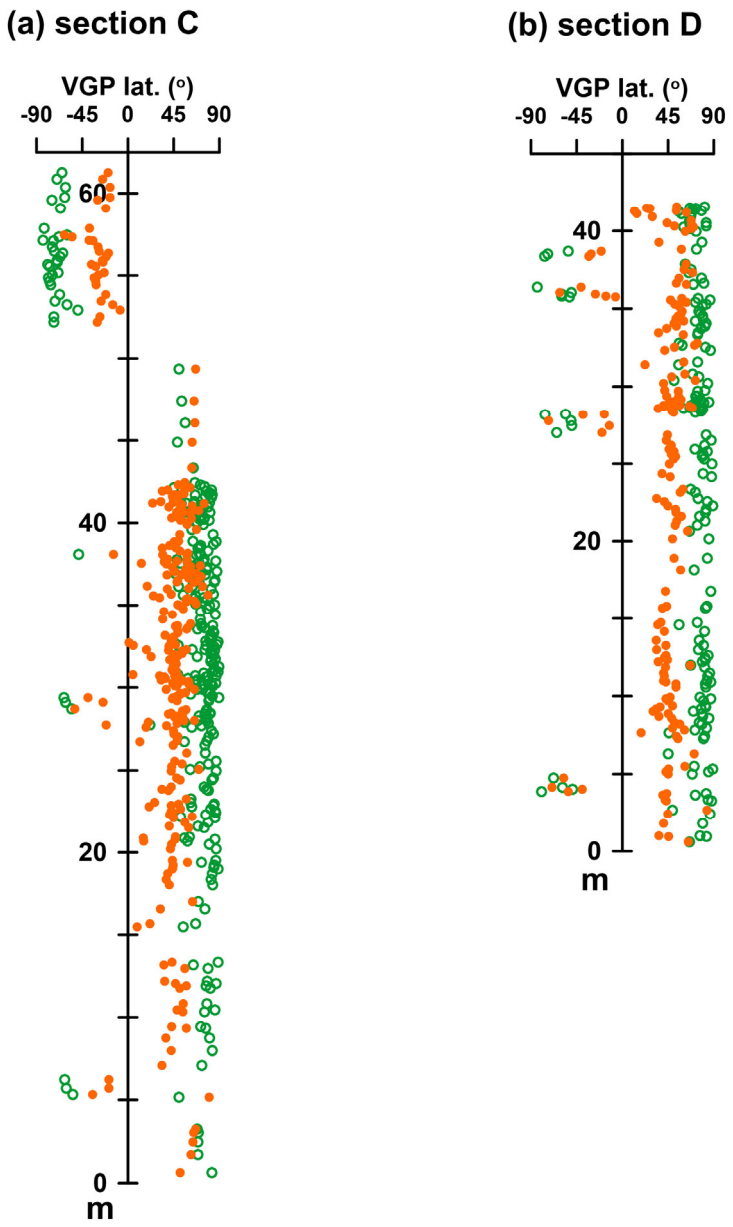

Figure S7. The specimen level VGP latitudes of the sampling location (orange) and the coordinates system where the mean P_3-T_1 paleomagnetic pole of SCB as a geographic pole (green). The latter were used for constructing the magnetozones. VGP = virtual geomagnetic pole, lat. = latitude.

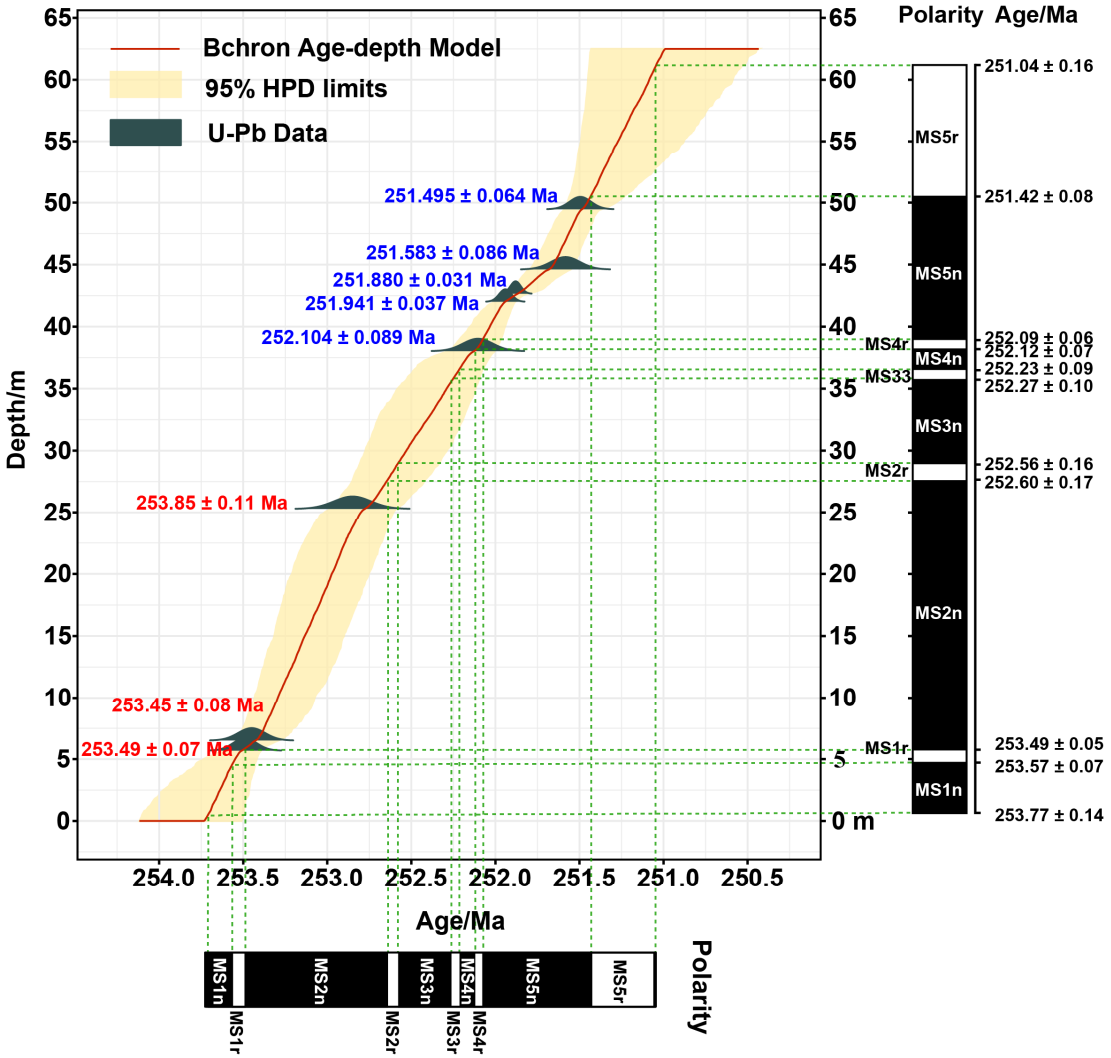

Figure S8. The Bayesian age-depth model for calculating the age and duration for each magnetozone of the Meishan section by using Bchron package (Haslett and Parnell, 2008; Parnell et al., 2008). The U-Pb data are from S.Z. Shen et al. (2011) (red fonts) and Burgess et al. (2014) (blue fonts), respectively.

Table S1: Collective paleomagnetic poles from the South China Block

Period	Age (Ma)	Lithology, location	Sites		Poles			Reference
			°E	°N	°E	°N	A_{95}	
P3-T1	252~251	Mud-limestone, Guizhou	105	26	214.6	46.2	2.7	(Glen et al., 2009)
		Limestone, Sichuan	105	32	218.8	44.1	2.4	
		Limestones, Sichuan	/	/	217.4	44.3	3.5	(Heller et al., 1995)
		Limestones, Sichuan	107	30	216.2	39.8	3.8	(Enkin et al., 1992)
		Limestones, Sichuan	/	/	223.6	46.1	2.7	(Steiner et al., 1989)
		Limestones, Sichuan	105	32	225.1	47.9	3.9	(Heller et al., 1988)
Mean position of poles					**219.2**	**44.8**	**3.4**	/

Note: ºE and ºN, longitude and latitude.

Table S2: Sampling information and ChRM directions of fold test.

Specimen Name	Strike (°)/Dip (°)	Dg (°)	Ig (°)	Ds (°)	Is (°)	MAD
F1	324/58	68.4	34.1	29.4	28.1	8.2
F2	328/58	89.7	41.1	27.9	42.1	11
F3	328/58	98.8	32.5	41.5	48.2	9.8
F4	328/58	80.6	30	39.5	32.5	6.9
F5	328/58	89.2	29.7	42.7	39.6	5.9
F7	351/20	35	55.4	20.6	38.8	7
F8	351/20	61.2	47.6	43.5	38.1	6.6
F9	327/31	98	35.1	71.9	50.3	13.4
F10	328/31	69.5	54.4	28.2	49.5	6.7
F11	328/31	75.4	53.7	32.5	51.9	6

Note: Dg/Ig & Ds/Is, declination and inclination before in situ and after tilt correction.
MAD, maximum angular deviation.

386 **Table S3: The ChRM directions of Meishan Section C**

ID	Depth (m)	NRM (10^{-4}A/m)	T (℃)	n	Dg	Ig	Ds	Is	MAD	Plon.	Plat.
C0301a	0.64	0.96	240~360	6	77.9	43.7	41.9	37.6	7	214.4	51.3
C0404	1.73	2.42	240~340	6	53.5	48.4	24.6	27.7	6.6	240.1	62.2
C0407	2.48	0.02	320~380	4	57.6	47	24.6	32.3	6.4	235.2	63.9
C0409	3.05	0.63	220~360	8	64.9	53.6	25.5	36.6	7.6	228.7	64.7
C0501	3.25	2.12	260~340	5	67.9	55.9	24.5	39.3	2.9	225.7	66.5
C0507	5.15	1.21	260~380	7	49.2	68.1	5.1	39.3	6.9	271.2	80.1
C0601	5.32	0.17	260~380	7	200.8	2.5	209.8	30.4	13.3	84.3	-34.6
C0604	5.69	12.30	380~460	5	228.9	10.8	240.3	20.5	8.2	55.3	-18.8
C0609	6.22	7.36	280~400	7	234.6	7.8	242.8	14.6	3.1	51.0	-18.8
C09l01	7.06	0.63	260~400	8	93.3	32.1	63.3	39.7	7.3	201.8	33.6
C09l05	7.96	2.34	260~460	10	82.9	36.6	51.8	36.1	4.5	210.2	42.4
C09l06	8.71	0.77	260~440	10	82.3	30.9	56.6	31.9	3.6	210.9	37.1
C09l09	9.29	4.97	280~400	6	79.7	50.1	35.9	42.1	7.6	212.8	57.6
C09l10	9.4	0.09	220~420	11	100.8	42.9	55.8	51	5.4	193.6	42.9
C10l01	10.32	0.66	240~400	9	91.1	49.4	41.9	48.3	6.4	201.5	54.0
C10l02	10.46	2.75	240~440	11	67.9	37.1	42	27.5	5.1	223.2	48.2
C10l04	10.83	7.76	240~380	8	85.3	48.7	40.2	44.5	6.7	207.4	54.6
C11l01	11.77	0.95	280~340	4	61.6	37.8	37.5	24.4	8	229.2	51.0
C11l02	11.92	0.09	240~380	8	80.1	49.8	36.4	42.2	7.5	212.3	57.2
C11l03	12.04	1.95	240~380	8	76.4	38.8	45.7	33.6	5.3	215.8	46.9
C11l04	12.2	0.96	240~380	8	85.3	31.1	58.5	34	7.9	208.4	36.1
C11l07	12.96	0.37	240~360	7	75.7	47.4	36.9	38.5	4.3	216.6	55.8
C11l08	13.19	0.48	280~400	7	107.8	38.8	66	53.2	5.2	188.1	35.2
C11l09	13.35	2.30	300~380	5	72.2	33.5	47.7	27.5	1.3	219.3	43.5
C12l03	15.48	2.98	280~460	8	72.4	-10.1	77.8	-4.9	9.8	218.2	9.1
C12l04	15.68	0.66	220~360	8	64.7	1.9	64.2	-0.6	9	224.0	21.7
C12l08	16.56	0.32	240~360	7	82.6	25.3	61.4	28.3	3	210.8	32.0
C13l02	17.02	0.26	240~360	7	58.8	51.3	24.9	32.3	6	234.8	63.7
C13l05	18.03	1.62	320~400	5	80.9	34.1	52.8	33.1	10.3	212.1	40.7
C13l07	18.36	0.58	320~380	4	77.9	29.3	54.9	28.1	5.7	214.5	37.5
C13l08	18.7	0.10	280~400	7	65	25.1	49.1	17.2	6.2	224.9	39.3
C13l09	18.98	1.39	280~440	9	71.3	33.4	47.2	27	4.8	219.9	43.7
C13l10	19.09	1.27	260~400	8	81.3	37.8	49.7	35.8	4.1	211.6	44.1
C13l11	19.23	0.77	260~400	8	80.6	37.8	49.3	35.5	3.2	212.1	44.4
C13l12	19.39	0.32	220~340	7	91.1	53.1	36.7	49.8	11.5	200.9	58.6
C13l13	19.5	3.22	220~360	8	66.7	31.4	45.7	22.8	6.3	223.9	43.8

C13l15	20.21	6.19	240~460	12	75	33	49.9	28.9	10.6	216.9	42.0
C13l16	20.48	1.04	240~460	11	88.2	38.9	52.8	40.8	7.3	205.6	42.8
C13l17	20.68	5.54	240~460	11	51.1	-13.8	64.1	-21.3	2.5	233.3	15.6
C13l18	20.79	3.49	220~400	11	77.3	36.3	46.8	35.5	2.4	213.5	46.5
C13l19	20.87	0.44	280~440	10	97.3	12.5	82.3	31.2	10.9	198.8	15.0
C13l20	20.95	5.14	300~500	12	26.4	14.8	25	-10.1	12.8	261.9	46.7
C13l23	21.5	0.84	220~380	9	66.8	45.9	31.4	35.4	7.1	224.4	59.5
C13l24	21.6	1.33	220~420	11	38.2	10.6	37	-7.2	9.2	247.5	40.5
C14l01	21.83	0.71	220~420	11	73.5	44.3	36.7	38.2	12.2	217.0	55.9
C14l03	22.11	11.60	240~500	12	77.7	34.6	48.6	34.6	3.1	213.2	44.7
C14l4a	22.2	0.92	240~460	12	22.8	41.5	8.7	11.3	10.8	280.1	63.3
C14l05	22.3	1.43	240~400	9	49.7	17.1	42	4.8	13.6	237.2	41.1
C14l06	22.43	6.18	240~460	12	76.7	33.9	48.6	33.6	7.9	214.0	44.4
C14l07	22.52	9.20	280~460	10	75.6	31.4	50.1	31.2	7.2	215.1	42.5
C14l8b	22.65	8.94	280~440	9	63.2	36.5	37.7	27.2	5.5	226.8	51.7
C14l09	22.8	1.87	420~500	5	48.4	-10.8	58.9	-17.7	8.1	234.9	20.8
C14l10	22.88	0.26	260~460	9	79.4	32.9	51.3	34.6	5.1	211.7	42.4
C14l11	22.97	1.81	260~400	8	73.4	38.1	42.7	34.3	5.6	217.0	49.7
C14l12	23.06	3.37	260~480	12	36.1	-9.7	48.2	-24.7	5.3	245.7	26.1
C15l01	23.27	0.28	160~360	12	33.4	33.7	20.1	9.2	6.1	260.1	57.5
C15l05	23.8	0.82	300~420	7	85.5	32.9	55.5	38.4	7.2	206.4	39.9
C15l06	23.87	0.82	220~380	9	79	22.6	59.6	27.2	8	212.4	33.2
C15l07	23.99	0.31	220~420	11	93	38.2	55	46.6	7.4	198.9	42.5
C15l10	24.41	0.93	280~400	7	77	41.1	42	38.3	8.6	213.6	51.4
C15l11	24.54	0.62	280~400	7	62.9	31.9	41.2	23.7	5.9	226.6	47.7
C15l12	24.97	0.10	260~400	8	67.4	27.7	47.4	23.5	1.7	222.2	42.5
C15l13	25.07	0.86	280~400	7	50.5	53.4	16.5	32.1	13.8	248.3	69.7
C15l14	25.22	4.88	260~400	8	40.4	15	36.2	-2.4	4.9	246.0	42.9
C15l15	25.39	0.64	200~360	9	81.9	44.3	41.2	43.2	7.1	208.5	53.4
C15l16	25.54	0.84	200~400	11	75.7	35	46.9	33.6	6.4	215.0	45.9
C1501	26.05	0.76	280~400	7	78	47.4	35.7	42.5	5.5	212.3	57.9
C1505	26.51	0.32	280~360	5	92.5	39.7	52.8	47.1	11.3	199.1	44.5
C161a	26.72	5.28	300~520	11	87.5	1.6	81.2	16.7	4.8	206.8	11.9
C1602	26.78	0.57	300~440	8	89.1	42.1	47.9	46.3	9.9	201.9	48.4
C1604	27.04	0.52	300~460	9	85.7	41.6	46.4	43.9	9.3	205.3	49.1
C1605	27.19	0.84	300~420	7	80.3	36.1	48.9	37.2	8.4	210.8	45.2
C1606	27.39	0.86	300~460	9	83.3	36.7	50.2	39.5	7.1	208.0	44.7
C1607	27.59	0.75	300~460	8	76.8	2.2	72.3	10.5	8.9	214.4	17.9
C1609	27.84	0.05	300~400	6	86.9	41.3	47.5	44.5	9	204.1	48.3

C1610a	27.99	3.34	300~400	6	82	46	39.2	44	6.5	208.5	55.3
C1611a	28.14	1.42	300~420	7	85.4	45.9	41.1	46.1	9	204.8	54.2
C1612a	28.29	0.21	300~400	6	99.9	43.8	51.9	54	6.1	190.7	46.7
C1613	28.44	2.30	280~420	8	84.4	35.2	52.5	39.3	8.1	207.1	42.7
C1614	28.59	1.15	280~440	7	86.2	45.6	42	46.4	4.9	204.1	53.5
C1616	28.65	0.68	280~380	6	69.9	44.3	34.7	36.1	13.7	220.8	57.0
C1620	29.38	3.05	300~440	8	288.2	-40.7	242.3	-57.6	8.3	3.6	-39.2
C1622	29.88	1.04	340~440	6	62.7	51.1	24.3	36.3	5.8	230.5	65.6
C1624	30.17	0.16	300~440	8	82.4	40.3	45.9	41.1	3.9	208.6	48.8
C1625	30.31	1.18	300~460	9	82.5	40	46.3	41	4.8	208.5	48.5
C1626	30.41	0.55	340~420	5	82	45.1	40.4	43.6	14.4	208.4	54.2
C1627	30.67	0.85	320~480	9	86.8	42.3	46.2	45	6.5	204.1	49.6
C1628	30.71	0.13	320~500	10	99.8	30.8	68.4	46.3	11.5	194.2	31.2
C1901	31.71	22.80	280~440	9	76.8	36.4	46.4	35.2	6.1	214.0	46.8
C192b	31.93	1.24	280~440	9	75.7	38.6	43.6	36	5.9	214.9	49.4
C1903	32.05	0.99	280~400	7	70	40.4	38.4	33.7	13.5	220.5	53.1
C1904	32.29	5.39	280~440	9	73.4	0.2	70.9	6.8	7	216.8	18.1
C1905	32.54	2.17	280~500	12	90.4	36	55.7	43.6	4.5	201.7	41.1
C1906	32.79	2.21	280~500	10	91.3	37.9	54.1	45.3	8.5	200.6	42.9
C1915	34.61	2.11	320~480	9	97	35	62.8	44	8.4	198.4	35.2
C1916	34.77	7.09	240~420	10	85.1	48.5	40.3	44.3	5.7	207.6	54.4
C1917	34.98	3.62	240~420	10	86	44.9	45	43	10	206.9	50.1
C1918	35.09	1.89	240~340	6	60.6	55.2	22.2	35.6	4.6	234.1	67.0
C1919	35.25	1.16	240~420	10	61	53.8	23.6	34.9	8.9	233.2	65.7
C2001	35.37	0.19	240~400	9	73	47.8	35.2	37.2	7.3	219.2	56.9
C2002	35.47	0.93	240~380	8	58.5	10.7	53.8	2.3	9.1	229.3	31.1
C2003	35.57	58.00	240~580	18	91.3	21.9	70.7	31.5	3.7	204.2	25.0
C2004	35.67	2.48	240~400	9	81.1	36.2	51.1	34.8	9.1	211.7	42.6
C2006	36.02	0.65	200~400	11	42.5	42.1	22.7	18	8.2	250.8	59.6
C2007	36.16	3.49	280~560	15	79.9	7.7	72.1	13.5	12.9	213.1	18.8
C2009	36.41	2.45	240~380	8	77.5	55.8	28.3	43.9	5	214.8	64.6
C211b	36.52	0.75	240~360	7	77.2	59.3	23.8	45.3	8.1	215.3	68.8
C2102	36.67	0.09	240~380	8	99	55.5	35.8	55	8.4	191.5	59.9
C213a	36.76	1.50	240~380	8	92.7	63.4	21.4	53.6	8.3	194.3	71.7
C2104	36.85	2.29	260~380	7	108	41.5	62.3	54.8	5	187.2	38.6
C2105	37.05	0.72	260~360	6	75.7	37.8	46.2	32.5	6.5	216.4	46.2
C2106	37.17	0.66	260~380	7	79	49.2	36.7	41.3	9.2	213.3	56.8
C2107	37.31	0.82	240~380	8	92	41	52.8	44.4	7.1	202.0	43.8
C2201	37.62	6.15	240~540	16	47.6	41.6	26.1	20	6	244.7	58.1

C2203	37.8	0.71	240~400	9	13.8	34	7.1	-0.3	12.2	286.2	58.1
C2204	38.06	0.73	280~400	5	102.6	36.1	65.6	48.4	9.2	193.2	34.2
C2206	38.48	0.94	280~340	4	101.2	46.5	50.9	53	1.7	192.3	47.3
C2207	38.62	0.15	240~340	6	100.1	41.3	57.5	49.7	7	194.6	41.2
C2208	38.7	1.36	240~420	10	81.4	40.3	47.3	37.5	5.3	211.4	46.7
C2209	38.86	1.18	320~420	6	77.5	38	47.2	33.8	9.7	214.7	45.7
C2210	38.9	4.32	300~440	8	32	24	25.7	-2	13.3	257.6	49.7
C2212	39.3	0.60	300~400	6	75.1	42.6	41.5	35.3	5.6	216.9	51.0
C2214	39.6	0.05	240~360	7	49.2	53.8	18.2	29.6	7.9	248.1	67.5
C2302	39.9	1.27	260~400	8	86.5	52.1	36.4	46.9	4	205.6	58.4
C2303	40.03	2.20	240~400	9	99.4	54.7	37.2	54.9	8.4	191.6	58.8
C2304	40.17	1.83	240~400	9	84.3	46.2	42.7	42.6	5.6	208.5	52.0
CB2401	40.22	5.19	280~440	9	94.3	48.7	44.4	49.7	5.7	198.7	52.1
CB2402	40.25	0.68	240~360	7	58.1	49.6	26	30.8	9.5	235.2	62.3
CB2404	40.28	3.36	240~400	8	80.5	54.5	31.1	44.8	9.7	211.6	62.4
C2305	40.3	1.04	260~400	8	95.1	41.3	54.4	46.5	6.9	199.2	43.0
CB2408	40.37	3.66	320~420	6	101.3	47.3	49.8	53.4	17.1	192.0	48.3
C2306	40.63	1.97	260~380	7	86.9	43.1	47.6	42.5	7.1	206.3	47.7
C2308	40.68	1.16	260~380	7	60.3	50.3	26.5	32.3	13	232.9	62.4
CB2411	40.75	3.17	280~420	8	84.7	60.8	23.8	49.4	16.6	205.8	69.6
CB2412	40.8	2.80	300~400	6	105.2	49.8	47.5	56.7	13.6	187.4	50.6
CB2413	40.95	3.66	320~400	5	88.8	36.7	55.6	39.9	4.1	205.1	40.2
C239c	41.04	0.88	240~320	5	81.9	55.1	30.7	45.8	9.5	210.1	63.0
C2401	41.1	0.66	240~400	9	94.4	49.7	43	50.3	5.3	198.2	53.4
CB2415	41.15	0.35	300~420	7	34.2	28.1	25.2	2.6	13	256.1	51.9
C2402	41.18	1.50	240~380	8	106.4	67.2	14.5	59.4	7.8	167.8	75.1
CB2417	41.2	0.90	340~400	4	110.5	30.9	78.2	50	14.8	187.2	24.5
CB2420	41.25	0.84	320~380	4	87.8	40.3	51.1	41.4	14.4	205.8	44.5
C2405	41.3	0.41	300~420	7	104.4	35	68.2	48.8	8.2	191.9	32.2
CB2423	41.56	1.57	340~400	4	83.8	42.8	46.2	40.4	3.6	209.1	48.4
C2408	41.6	2.09	280~420	8	94.4	41.8	53.4	46.3	8	199.8	43.8
CB2426	41.7	0.95	340~400	4	107.8	50	48	58.3	18	184.6	50.4
C2409	41.72	0.14	300~400	6	83.6	40.3	48.6	38.8	11.5	209.5	45.9
C2410	41.77	0.98	260~380	7	71.8	45.9	36.5	35.4	16	220.2	55.2
CB2431	41.83	0.05	300~400	6	74.7	45.9	38.1	37.1	6.9	217.3	54.4
C27R3	41.93	16.60	340~500	8	59.2	15	51.7	5.9	12.4	229.1	33.8
C27R4	41.99	23.10	340~440	6	62.9	24.1	48.4	15.1	7.4	226.6	39.2
C29R1	42.13	1.25	220~500	12	11.3	40.1	2.9	4.7	8.4	293.7	61.1
C29R2	42.21	2.02	220~400	10	56.9	42.2	31.5	25.1	16.5	234.3	56.0

C29R3	42.3	2.69	300~440	8	42.6	28.4	31.3	7	11.7	246.5	49.6
C29m15	42.45	0.85	300~400	6	38.2	35.4	24	10.5	14.4	253.7	55.8
C3202	43.34	5.07	260~380	7	43.2	46.4	20.3	21.7	9.2	251.8	62.7
C3401	44.89	7.14	260~500	12	17.2	43.3	5.8	9.4	9.1	286.8	63.1
C3403	46.07	10.50	260~480	11	32.3	48.8	12.5	19.2	14.1	268.3	65.8
C3406	47.42	17.90	260~480	14	25.2	46.7	9.4	14.9	11.1	277.3	64.9
C349a	49.37	11.60	260~540	15	22.4	49.2	6.4	16.2	8.6	283.7	66.4
C3701	52.19	4.88	320~600	15	237	-8.8	233.9	0.2	10.1	50.4	-30.2
C3702	52.51	2.91	360~540	7	250.1	-13.2	241	-11.5	12.9	40.3	-27.7
C3703	52.91	0.37	300~380	6	279.7	-7.1	268.7	-25.4	8.8	18.9	-7.9
C3705	53.25	2.90	280~560	14	243.7	7.6	249.7	8.5	14.8	44.2	-14.9
C3706	53.45	8.05	420~600	10	249.5	-11.4	241.8	-9.6	5.4	40.7	-26.5
C3708	53.85	4.90	420~600	10	252.5	-7.1	246.8	-8.3	7.9	38.4	-22.0
C3711	54.44	0.09	480~580	6	258.8	-22.7	240.7	-24	11.1	33.8	-31.4
C3712	54.65	0.97	480~600	7	251.4	-19.3	237.8	-16.8	13.4	39.5	-31.9
C3801	54.86	0.75	380~600	10	247.5	-18.9	235.2	-14.1	14.5	42.5	-33.3
C3802	55.03	0.43	380~540	9	253.2	-17	240.7	-16.2	9.4	38.1	-29.3
C383b	55.17	1.09	380~560	10	253	-9.5	245.7	-10.5	17.5	38.0	-23.5
C3805	55.54	2.58	340~580	11	249.7	-18.3	237.2	-15	5.4	40.8	-31.9
C3806	55.68	1.46	380~580	9	241.1	-19	230.5	-10.2	11.8	47.7	-36.1
C3807	55.81	4.99	340~580	13	247	-7.1	242.7	-4.7	8.3	42.5	-24.4
C3808	55.9	2.96	420~600	12	257.8	-14.5	245.9	-17.3	8.6	34.6	-25.1
C3810	56.15	1.46	360~500	7	255.2	-8.2	248.1	-10.9	13.8	36.5	-21.6
C3811	56.35	2.93	360~580	13	255.1	-5.1	250.2	-8.5	6.7	36.4	-19.1
C3812	56.47	1.66	380~560	9	241.1	-8.8	237	-2.4	13.6	47.1	-28.5
C3901	56.72	0.03	320~500	9	245.7	-12.9	237.8	-8.3	15	43.8	-29.5
CB2	57.1	1.83	400~580	8	265.9	-20	242.4	-39.4	16.9	22.5	-34.3
CB3	57.12	0.14	300~380	4	248	-15.1	232.3	-23.6	4.6	38.9	-38.5
CB5	57.35	0.04	300~440	6	220.4	-24.2	206.2	-11.9	16.1	69.9	-54.9
CB6	57.45	2.05	300~520	9	216.1	-33.9	196.5	-16.3	6.9	82.2	-62.5
CB10	57.85	0.44	380~600	7	242.7	-11.7	230.9	-17.9	9.7	43.3	-38.0
CB19	59.07	0.36	340~480	9	255.7	0.6	249.6	-17.4	14	32.5	-22.0
CB27	59.6	0.76	320~540	8	247.4	-6.5	239.2	-13.3	9.9	40.5	-29.7
CB22	59.77	0.95	320~440	4	237.4	17.3	246.8	7.1	14.2	45.3	-17.7
CB28	60.38	1.17	320~480	8	262.4	-0.1	255	-19	15.8	28.9	-17.8
CB32	60.88	0.08	300~520	11	255.1	-4.7	246.1	-17.5	14.9	34.3	-25.0
CB34	61.27	0.43	280~400	7	250.5	4.6	249.3	-7.5	5.3	37.4	-19.6
BC1601	27.7	0.73	300~420	7	98.1	38.1	60.1	46.6	5.5	197.0	38.2
BC1603	27.91	1.56	320~500	10	108.3	25.9	81.6	45.1	10.6	190.0	20.1

BC1604	28	1.13	340~420	5	66.3	54.7	25.1	37.8	9	227.4	65.5
BC1605	28.2	0.21	340~400	4	91.4	42.7	50.4	45	6.9	202.4	46.0
BC1606	28.4	0.86	240~380	8	93.3	38	57	43.6	11.1	201.1	40.0
BC1607	28.45	0.81	340~460	5	71.1	44.6	37.3	34.3	7	220.8	54.2
BC1608	28.7	0.82	340~420	4	201.4	-24.5	197	6.1	4.2	91.2	-52.2
BC1609	29.1	14.60	240~600	16	283	-27.5	255.3	-42.9	6.8	14.3	-24.5
BC1610	29.2	1.16	280~440	8	88.6	44	47.4	43.9	7.4	204.8	48.3
BC1612	29.31	1.48	260~460	9	87.9	39.8	51.7	41.2	9.9	205.7	43.9
BC1613	29.38	0.80	280~420	8	73.1	34.8	47.1	28.9	13.4	218.6	44.4
BC1614	29.49	2.75	280~440	8	82.3	42.5	45.6	39.4	4.9	210.5	48.6
BC1615	29.59	0.61	300~360	4	29.6	26.4	22.5	-0.9	7	261.4	51.9
BC1616	29.64	1.31	260~420	9	83.4	45.3	43.1	41.6	6.6	209.4	51.4
BC1617	29.69	0.53	220~380	9	72.8	47.4	35.5	36.9	6.4	219.4	56.5
BC1618	29.89	0.54	260~440	10	47.4	13.4	43.7	-2.4	14.3	239.2	37.5
BC1619	30.09	1.71	240~400	9	82.8	40.7	47.8	38.6	9.3	210.1	46.5
BC1620	30.19	0.94	220~400	10	85.8	53.6	34.2	47.1	8.4	206.3	60.3
BC1621	30.27	0.73	220~420	10	78.2	36.6	48.9	33.2	4.6	214.2	44.1
BC1622	30.36	3.13	260~420	9	44.6	42.9	23.5	19.5	6.6	248.6	59.7
BC1623	30.44	0.99	300~400	6	100	33.8	66.4	45.1	10.7	196.0	32.5
BC1624	30.53	1.70	260~540	15	26	2.7	31.9	-23.2	4.6	259.3	37.1
BC1625	30.64	3.51	300~420	7	87.4	31.4	59.7	35.6	5.5	206.6	35.5
BC1626	30.71	1.30	280~400	7	67.8	34.9	43.8	25.8	3.2	223.2	46.2
BC1627	30.78	1.91	320~580	14	55.5	-24.8	75.6	-26.6	7.8	229.2	4.7
BC1628	30.86	0.44	260~440	10	96.4	44.7	50.8	49.1	12.2	197.5	46.6
BC1630	30.93	1.37	200~420	12	70.5	34.4	45.8	27.1	5.3	220.8	44.9
BC1631	30.99	1.50	260~440	10	81.9	41.2	46.6	38.4	5.7	210.9	47.5
BC1632	31.05	0.14	240~460	12	78.8	35.9	49.9	33.1	5.8	213.7	43.2
BC1633	31.26	3.43	260~460	11	71.7	34.4	46.6	27.9	4.6	219.7	44.5
BC1634	31.41	0.99	260~460	11	64.2	34.9	41.4	23.8	4.4	226.4	47.6
BC1635	31.57	0.70	260~440	10	86.3	40.3	50.2	40.5	4.8	207.1	45.0
BC1637	31.66	3.67	260~440	10	84	35.7	53.4	36.2	3	209.3	41.1
BC1901	31.86	0.82	200~420	12	70.2	7	65.2	6.8	4.2	220.0	22.9
BC1902	31.99	6.08	220~520	16	84.3	39.2	50.1	38.6	7.3	208.9	44.6
BC1903	32.19	0.48	260~480	12	76.1	45.1	39.5	37.3	11.3	216.2	53.3
BC1904	32.23	12.50	320~440	7	72.4	29.5	50.9	24.9	18.4	219.0	40.0
BC1905	32.28	5.37	240~420	10	83.5	50.8	36.9	44.7	7.6	208.7	57.4
BC1906	32.47	1.01	280~440	9	77.3	32.1	52.2	29.7	8.4	214.9	40.3
BC1907	32.55	9.90	500~600	6	55.8	-23.9	75.2	-25.8	8.9	229.0	5.2
BC1908	32.6	0.48	300~460	9	74.3	38	45.2	31.8	4.7	217.6	46.8

BC1909	32.7	16.50	240~600	19	57	-28.2	79.4	-28	3.3	227.9	1.1
BC1910	32.75	0.46	280~480	11	71.8	33.6	47.3	27.3	8.4	219.7	43.7
BC1911	32.87	2.71	280~460	10	87.5	38.6	52.8	40.2	6.3	206.1	42.7
BC1912	33.04	0.12	300~420	7	86.1	39.9	50.5	40.2	3.3	207.2	44.6
BC1913	33.14	6.84	340~480	7	75.3	26.8	55	24.7	11.7	216.6	36.5
BC1915	33.31	3.58	240~460	12	78.4	41.6	44.2	36.5	7.3	214.1	49.0
BC1916	33.4	4.36	280~440	9	80.3	42.4	44.6	38.1	6.1	212.3	49.1
BC1919	33.52	9.60	240~440	11	44.9	40.3	25.4	17.7	14.4	247.3	57.7
BC1920	33.61	0.49	300~420	7	68.5	48.3	32.3	35.2	7.4	223.8	58.7
BC1921	33.69	3.70	340~480	8	99.5	45.5	51.4	51.4	6.2	194.4	46.6
BC1922	33.74	19.80	260~440	10	63.5	36	40.1	24.2	11.8	227.2	48.8
BC1923	33.87	0.89	260~420	9	62.6	49.9	28	33.2	4.8	230.2	61.6
BC1924	34.13	0.91	300~540	13	96.5	33.8	63.7	42.9	5.5	199.0	34.2
BC1925	34.43	3.77	280~480	11	78.3	36.2	49.3	33	3.3	214.1	43.7
BC2001	35.03	15.20	300~520	12	68.6	38.1	41.6	28.6	7.3	222.6	48.9
BC2002	35.23	2.83	300~400	6	88.1	51.9	37.3	47.7	3.6	204.1	57.7
BC2003	35.41	3.68	300~420	7	105.8	55.5	37.4	58.7	11.5	183.9	58.6
BC2005	35.62	0.55	260~460	11	91	68.3	12.9	53.6	13.1	190.5	78.7
BC2010	35.99	5.69	240~440	11	80.6	31.7	54.7	31.5	10.1	212.2	38.6
BC2011	36.15	1.27	280~440	8	34.5	58.2	4.8	28.4	13.8	283.2	73.5
BC2012	36.43	0.04	260~380	7	65.7	33.3	41.4	26.1	8.7	224.7	48.3
BC2013	36.53	3.72	260~420	9	72.6	36.7	42.8	32.6	7.9	218.5	49.1
BC2015	36.78	0.68	200~400	11	45.9	39.7	24.3	19.5	14.7	247.5	59.2
BC2016	36.86	0.74	200~400	11	54.7	34.9	33.2	20.7	11.5	236.0	53.1
BC2018	36.95	0.97	180~420	13	20	50	2.4	16.9	6.6	293.5	67.4
BC2201	37	1.12	200~400	11	71.3	49.4	29.4	39.4	7.4	221.0	62.4
BC2202	37.22	8.15	260~380	7	96.2	50.2	38.9	54.1	15.1	192.9	57.3
BC2203	37.35	0.45	280~480	11	53.3	44.7	24.7	26.9	17.6	240.8	61.8
BC2204	37.4	3.12	240~400	9	58	55.6	17.2	36.1	7.6	241.2	71.0
BC2205	37.5	0.36	260~380	7	102.3	36.8	62.1	51.7	14.8	190.9	37.9
BC2207	37.55	1.88	260~360	6	33.9	-24.8	58.9	-37.4	10.8	244.5	13.2
BC2208	37.65	6.43	300~440	8	90.2	29.9	60.9	39.5	15.6	203.1	35.6
BC2209	37.69	2.08	260~400	8	70.8	35.2	43	30.5	9.6	220.1	48.3
BC2211	37.82	1.57	320~480	8	92.3	34.2	58.1	43.6	9.1	200.7	39.1
BC2212	38.1	1.91	220~400	10	205.5	25.9	233	43.6	8	71.7	-14.1
BC2215	38.1	10.30	280~460	10	91.8	49.7	37.9	51.3	8.5	198.0	57.8
BC2216	38.16	4.68	280~440	9	93.3	50.9	36.7	52.6	13.6	196.0	59.0
BC2217	38.3	0.43	300~420	7	57.4	33.5	36	21.3	13.3	232.8	51.2
BC2219	38.46	1.60	300~440	8	98	31.6	65	45.8	12.6	195.9	33.9

BC2706	40.65	90.20	300~380	5	25.2	28.5	16.9	0.5	17.9	269.0	55.3

387

388 **Table S4**: the ChRM directions of Meishan Section D

ID	Depth (m)	NRM (10^{-4}A/m)	T.R. (℃)	n	Dg	Ig	Ds	Is	MAD	Plon.	Plat.
D0301	0.61	8.66	280~360	5	49.6	53.4	21.7	29.1	9.7	242.8	64.8
D0402	0.94	3.45	220~460	11	84.0	43.7	49.0	39.0	7.7	209.1	45.6
D0403	0.99	3.93	260~460	8	89.2	36.2	59.6	37.1	11.9	205.6	36.0
D0410	1.81	1.35	220~360	8	88.5	40.4	55.0	39.5	3.7	205.7	40.6
D0414	2.42	2.45	220~360	8	78.6	41.0	48.3	34.1	6.9	213.8	44.8
D0415	2.66	3.18	220~400	8	50.7	73.7	4.1	43.6	7.5	266.0	83.3
D0419	3.26	0.847	220~400	9	74.6	37.6	48.6	29.6	9.1	217.2	43.3
D0501	3.36	0.504	240~400	7	80.5	38.9	51.3	33.9	4.7	212.3	42.2
D0504	3.64	2.99	240~360	7	100.3	43.6	58.8	48.5	12.7	195.5	39.8
D0505	3.74	1.85	240~440	10	84.2	42.0	50.8	38.0	7.4	209.1	43.8
D0506	3.88	4	280~560	14	241.5	-43.6	215.8	-27.0	4.7	48.6	-53.2
D0507	4.01	6.56	280~460	10	194.1	-2.4	199.4	29.6	2.7	95.2	-39.5
D0508	4.14	5.38	280~580	14	219.0	-56.7	194.1	-28.0	5.4	78.0	-69.3
D0513	4.74	2.44	280~580	15	221.6	-41.9	204.6	-16.7	6.4	69.0	-57.9
D0515	5.01	2.52	280~380	5	106.4	49.5	54.0	55.0	8.0	188.9	45.2
D0601	5.14	0.938	280~460	10	63.7	32.1	45.5	19.6	10.8	226.1	43.0
D0603	5.33	25.1	280~460	10	70.4	38.2	45.5	27.7	11.9	220.6	45.4
D0604	5.5	6.12	240~440	11	55.3	51.1	26.6	29.8	7.1	235.5	61.4
D0801	6.31	2.02	260~440	5	14.0	58.0	0.3	22.6	16.9	298.8	70.7
D0808	7.27	2.46	240~380	8	75.4	49.9	38.1	38.3	9.8	216.0	54.7
D0809	7.42	6.95	220~380	7	78.0	49.1	40.2	39.1	6.0	213.8	53.2
D0902	7.66	2.85	300~400	6	123.4	33.9	89.8	56.4	11.3	177.0	18.2
D0903	7.83	1.5	280~400	7	86.6	58.1	33.3	48.2	4.4	204.8	61.3
D0904	7.96	6.09	260~400	6	80.9	46.5	44.4	39.0	12.9	211.5	49.5
D0905	8.2	0.594	300~360	4	73.4	51.0	35.9	38.0	12.9	217.8	56.5
D0906	8.31	1.28	200~360	9	93.7	51.3	45.4	48.7	8.5	199.8	51.1
D0908	8.57	1.77	220~400	9	66.9	40.4	41.6	27.4	5.3	223.6	48.5
D099b	8.69	0.876	240~400	6	83.6	33.7	57.9	32.1	9.8	210.1	36.1
D0911	8.89	6.39	240~440	10	91.4	45.6	51.2	44.3	6.5	202.8	45.1
D0912	9.04	3.52	240~400	9	94.1	32.2	66.6	37.4	4.2	202.1	30.1
D0913	9.17	1.64	280~340	4	80.0	28.7	59.5	26.5	2.6	212.9	33.1
D914b	9.29	8.69	260~400	8	76.5	31.5	54.7	26.4	7.2	215.7	37.2
D0915	9.38	2.22	200~360	9	84.1	47.1	45.5	41.1	10.3	208.8	49.2
D0918a	9.7	1.19	280~400	7	88.8	44.3	51.2	42.1	3.2	205.1	44.6

D0919	9.82	2.37	240~380	8	68.3	34.2	47.0	23.7	10.0	222.4	42.9
D0920	9.94	0.898	280~340	4	49.7	30.6	36.7	11.1	7.8	238.6	47.2
D1003	10.57	1.41	200~400	8	69.7	46.0	38.6	32.8	3.7	221.3	52.7
D1005	10.78	2.17	220~340	7	74.5	47.9	39.6	36.5	2.5	216.9	52.9
D1006	10.89	1.66	280~360	5	75.9	37.6	49.5	30.4	4.9	216.0	42.8
D1007	10.98	2.64	240~400	9	80.9	37.6	52.8	33.2	2.1	212.0	40.7
D1102	11.28	7.36	280~440	9	80.3	37.9	52.1	33.1	4.8	212.5	41.3
D113a	11.48	0.698	300~380	5	73.1	34.0	50.6	26.2	8.3	218.3	40.6
D115a	11.85	3.36	280~400	7	86.6	41.6	52.6	39.1	11.0	207.2	42.6
D1106	11.98	1.12	260~400	8	61.6	58.3	23.4	37.4	10.8	229.9	66.7
D1107	12.2	1.61	260~380	5	81.9	32.0	58.1	29.9	9.8	211.5	35.3
D118a	12.34	4.85	240~420	10	86.0	43.2	50.6	39.8	3.5	207.5	44.5
D1109	12.45	1.64	240~420	9	85.0	39.8	53.3	37.1	4.2	208.6	41.4
D1110	12.6	1.02	240~420	7	81.1	39.8	50.9	34.9	4.0	211.7	42.8
D1112	12.97	1.21	240~400	9	89.2	33.9	61.6	35.6	13.3	205.7	33.9
D1114	13.25	1.96	280~440	8	88.9	42.6	53.0	41.2	2.9	205.1	42.8
D1116	13.58	11.2	280~460	10	86.5	32.2	61.2	32.8	5.3	207.9	33.4
D1120	14.16	2.12	300~400	6	85.7	40.0	53.7	37.6	7.4	208.0	41.2
D1122	14.57	1.41	300~400	5	120.9	45.4	69.6	61.9	4.8	176.1	34.8
D1123	14.72	0.738	280~380	6	96.1	40.5	59.7	44.2	11.7	199.5	37.9
D1204	15.68	1.44	240~400	9	82.5	37.0	54.3	33.7	4.5	210.8	39.6
D1205	15.8	0.61	280~380	6	60.8	31.4	44.0	17.4	11.6	228.6	43.5
D1301	16.78	2.52	240~400	9	74.5	36.5	49.5	28.7	11.1	217.3	42.3
D1310	18.14	2.09	340~460	7	47.5	43.4	27.4	20.4	7.4	242.7	57.3
D1315b	18.91	2.58	320~440	6	74.8	46.0	41.5	35.4	9.4	216.8	51.0
D13182	20.16	1.54	200~380	10	74.0	44.1	42.8	33.8	5.1	217.4	49.4
D1320	20.66	0.441	200~400	11	47.6	51.9	21.8	27.2	9.3	244.6	64.0
D1322	21.04	0.364	200~380	9	47.6	36.3	31.9	14.7	6.3	241.4	52.0
D1323a	21.3	0.379	200~400	7	70.7	47.1	38.2	34.0	5.7	220.4	53.4
D1324	21.6	1.48	280~420	8	63.4	49.7	32.0	32.3	2.6	227.2	58.0
D1402	21.86	3.22	220~400	10	76.3	48.1	40.3	37.6	5.8	215.4	52.7
D143b	22.04	1.56	240~380	8	73.7	47.1	39.9	35.6	4.3	217.6	52.4
D1405	22.29	1.7	220~380	9	70.4	37.4	46.1	27.1	8.5	220.6	44.7
D1406	22.57	22.5	220~460	13	81.4	38.4	52.3	34.1	4.0	211.6	41.4
D1407	22.75	2.48	260~420	8	89.8	33.9	61.9	36.0	7.4	205.3	33.7
D1408	23.15	0.518	260~400	8	49.2	43.7	28.3	21.4	13.2	240.9	57.1
D1501	23.36	0.435	260~380	7	43.2	44.9	23.8	19.8	10.2	248.0	59.6
D154a	24.15	1.15	240~380	8	71.1	40.4	44.2	29.7	4.7	219.9	47.1
D155a	24.36	0.379	240~420	10	87.4	38.5	56.0	37.6	6.9	206.9	39.2

D1507	24.98	13.1	320~500	9	74.3	40.8	45.8	31.7	8.9	217.3	46.3
D1509	25.31	1.36	240~460	11	84.7	48.3	44.5	42.1	4.6	208.2	50.3
D1510	25.45	1	300~440	8	86.2	50.5	42.8	44.2	7.6	206.5	52.3
D1511	25.61	1.05	300~420	7	88.9	47.7	47.5	44.1	6.1	204.6	48.2
D1512	25.77	1.27	300~400	6	74.7	45.8	41.6	35.2	8.8	216.9	50.9
D1513	25.93	1.45	300~420	7	102.4	49.3	52.4	52.6	10.1	192.5	46.0
D1514a	26.19	2.88	300~440	8	86.4	46.8	47.0	42.2	4.0	206.9	48.2
D1516a	26.5	0.831	280~400	7	75.4	37.8	49.0	30.2	9.3	216.5	43.1
D1601	26.85	0.976	300~380	5	85.0	42.7	50.5	38.9	2.6	208.4	44.3
D1602	27.01	6.79	260~540	15	242.4	-0.7	244.2	6.0	7.9	46.4	-20.2
D1605	27.45	0.889	220~360	8	289.6	-22.2	268.2	-39.6	12.7	11.0	-12.8
D1606	27.77	4.45	260~540	16	205.7	-59.8	185.5	-27.0	5.5	101.7	-72.5
D168b	28.19	2.69	260~420	9	272.7	-40.2	237.9	-41.9	5.7	22.3	-38.8
D1609	28.34	2.09	320~400	5	100.2	52.4	46.8	52.8	10.0	193.6	50.7
D1610	28.52	1.67	320~440	5	89.5	47.8	47.6	44.6	9.3	204.0	48.3
D1612	29.02	1.1	240~420	10	75.3	44.1	43.5	34.5	7.8	216.3	49.1
D1614	29.39	1.39	320~420	6	93.2	54.9	40.4	50.0	4.9	199.5	55.5
D1615	29.71	0.934	320~400	5	92.7	54.2	41.0	49.5	9.6	200.0	54.9
D1616	29.76	0.337	320~380	4	85.2	40.1	53.2	37.4	10.0	208.4	41.6
D1618	30.2	1.58	300~420	7	79.4	36.9	52.4	31.9	4.3	213.2	40.7
D1619a	30.42	0.826	300~400	6	118.5	69.6	15.7	63.0	9.0	157.9	71.8
D1620	30.62	0.566	260~380	7	95.6	49.5	48.6	48.9	11.2	198.4	48.4
D1621	30.82	2.34	300~460	9	93.2	59.4	33.7	51.9	14.5	197.8	61.4
D1901	31.42	1.7	260~360	6	112.3	32.8	80.5	49.1	6.8	187.2	22.4
D1902	31.58	1.22	220~360	7	65.4	52.8	30.3	35.4	10.5	225.4	60.4
D1906	32.34	0.714	240~360	7	70.4	33.8	48.8	24.6	8.0	220.5	41.7
D1908	32.54	2.36	320~420	6	80.7	47.9	42.9	39.8	9.9	211.5	51.0
D1909	32.66	0.675	300~360	4	100.0	67.2	21.8	56.6	10.8	185.1	71.0
D1910	32.79	2.74	240~400	9	40.7	62.4	10.8	33.1	9.2	260.3	73.7
D1914	33.33	4.61	240~320	5	64.8	52.1	30.5	34.7	6.0	226.0	60.0
D1915	33.46	1.81	260~340	5	93.1	37.4	61.0	40.3	4.5	202.4	35.7
D1917	33.73	1.96	280~360	5	92.5	44.7	52.8	44.5	5.0	201.9	43.8
D1918	33.88	4.12	260~360	6	73.1	47.7	38.9	35.7	5.4	218.2	53.3
D1919	34.05	1.28	260~360	6	80.0	47.3	43.0	39.0	9.7	212.3	50.7
D1920	34.21	3.42	260~380	7	88.4	57.7	34.5	48.9	7.7	203.1	60.4
D1921	34.36	2.66	260~360	6	83.7	50.2	42.0	42.7	5.2	208.7	52.6
D1922	34.53	2.86	260~380	7	79.1	51.1	38.6	40.9	8.4	212.7	55.0
D1923	34.69	1.94	260~400	8	67.0	50.6	33.1	34.6	5.0	223.8	57.8
D1924	34.84	6.02	240~380	8	79.5	54.8	34.8	43.2	4.0	211.9	58.9

D1926	35.15	3.84	300~400	6	74.1	50.7	36.6	38.1	12.5	217.2	56.0
D1927	35.28	2.77	240~380	8	77.3	47.5	41.4	37.8	5.2	214.5	51.8
D2001	35.41	3.65	220~360	8	72.4	57.1	29.2	41.1	4.8	218.7	63.1
D2002	35.56	1.38	220~340	7	67.9	39.5	42.9	27.3	8.1	222.7	47.4
D2003	35.65	0.811	220~380	8	59.5	48.8	30.6	29.9	2.9	231.0	58.3
D2005	35.77	0.455	220~360	8	254.0	9.7	259.8	7.0	14.0	38.0	-6.9
D20051	35.81	0.528	260~380	7	268.0	-12.4	257.0	-19.0	15.6	27.9	-16.1
D20052	35.94	0.247	240~380	8	289.9	-35.4	255.5	-49.3	13.0	8.9	-26.4
D2006	36.04	3.29	300-420	5	307.6	-63.7	206.7	-68.4	9.4	335.6	-61.6
D2008	36.38	0.49	220~400	10	244.2	-29.6	227.5	-17.9	13.4	45.6	-40.8
D2102	36.56	1.28	260~380	7	86.3	59.6	31.3	48.7	6.0	204.6	63.0
D2103	36.64	0.534	260~360	6	80.9	49.9	40.9	41.1	12.3	211.2	53.1
D2105	36.96	0.455	300~360	5	80.5	52.3	38.0	42.1	13.0	211.6	55.9
D2108	37.32	0.715	240~340	6	81.0	63.6	24.2	48.1	7.3	208.8	69.0
D219a	37.5	2.76	240~340	6	97.6	59.6	34.5	54.1	6.5	193.4	60.9
D222a	37.87	0.662	280~360	5	108.1	62.0	32.1	59.5	11.1	181.1	62.5
D2205	38.36	0.35	220~320	6	263.0	-30.0	240.5	-29.1	2.4	30.8	-33.0
D2206	38.52	20.3	240~540	15	237.6	-12.3	233.4	-0.5	5.1	50.5	-30.9
D2207	38.68	5.56	280~480	11	210.2	15.8	226.8	38.1	5.9	73.1	-20.9
D2208	38.81	0.887	280~380	6	90.6	56.3	37.3	49.4	5.9	201.4	58.1
D2211	39.26	1	280~380	6	85.0	34.2	58.4	33.2	4.8	209.1	35.9
D233a	39.95	2.81	240~340	6	67.0	54.8	29.1	37.3	5.9	224.1	62.0
D2305	40.14	2.7	240~380	8	73.5	61.4	24.6	44.0	11.1	217.3	67.8
D2306	40.23	1.07	220~340	7	45.4	58.6	15.8	31.6	4.6	250.3	70.0
D2307	40.32	1.54	240~380	8	78.6	47.2	42.3	38.3	9.0	213.4	51.1
D2308	40.42	1.36	240~380	7	64.3	60.1	22.7	39.5	6.8	227.4	68.0
D2309	40.51	4.03	240~440	11	84.4	42.1	50.8	38.2	10.0	208.9	43.8
D2310	40.67	3.43	260~340	5	82.8	62.9	25.7	48.5	2.3	207.2	67.8
D2314	40.92	1.58	300~380	5	99.1	33.6	68.9	41.4	13.4	198.1	29.4
D2403	41.11	1.52	320~520	11	86.0	8.5	78.0	14.7	9.9	209.4	14.1
D2404	41.2	1.98	260~400	7	91.1	60.4	31.5	51.2	13.8	199.7	63.2
D2405	41.28	2.18	280~400	7	91.6	9.3	82.1	18.9	7.2	205.3	11.7
D2406	41.32	1.93	280~400	7	87.2	51.4	42.2	45.3	9.6	205.4	53.0
D2408	41.41	3.59	240~380	8	56.8	5.5	56.8	-5.4	11.2	230.8	26.4
D2409	41.45	1.05	240~380	8	78.0	20.5	63.9	19.0	7.4	214.8	27.3
D2410	41.5	1.85	240~420	10	90.0	23.0	71.1	28.3	4.4	205.9	23.7
D2411	41.55	2.8	260~380	7	76.0	48.9	39.3	38.0	5.9	215.6	53.6
BD1601	28.2	19.8	320~440	7	285.3	-25.2	261.9	-39.2	4.3	14.1	-17.9
BD1602	28.4	2.34	320~440	6	91.4	49.0	47.2	46.3	9.4	202.1	49.0

BD1603	28.58	1.67	320~460	7	115.3	44.3	67.5	57.9	15.8	182.0	35.3
BD1604	28.64	0.837	320~420	6	90.6	50.0	45.5	46.3	3.6	202.8	50.5
BD1605	28.69	1.79	320~440	7	100.7	44.0	58.5	48.8	6.9	195.3	40.1
BD1607	28.73	0.693	300~400	6	64.8	58.4	24.6	38.7	8.1	226.6	66.2
BD1608	28.81	1.29	300~400	6	73.0	51.0	35.6	37.8	6.3	218.3	56.7
BD1610	29.06	1.94	260~420	9	100.5	49.2	51.5	51.4	5.0	194.3	46.5
BD1611	29.17	2.46	280~420	8	70.9	51.8	34.0	37.2	8.5	220.1	57.9
BD1612	29.39	2.99	360~440	4	101.1	47.0	54.9	50.8	7.3	194.1	43.6
BD1615	28.64	0.889	340~440	6	71.5	61.9	23.5	43.4	16.4	219.4	68.5
BD1617	28.79	9.04	320~400	5	107.1	46.3	59.3	53.9	7.1	189.1	40.7
BD1618	28.96	1.33	240~460	11	77.4	49.7	39.3	39.1	7.1	214.4	53.9
BD1619	29.05	3.46	280~420	8	89.3	51.1	43.5	46.3	7.4	203.6	52.2

389 Note: NRM, nature remanent magnetization. T, temperature range of the ChRM
390 direction. n, number of selected demagnetization steps for ChRM. Dg/Ig and Ds/Is,
391 declination/inclination in geographic coordinates and stratigraphic coordinates,
392 respectively. Plon./Plat., longitude and latitude of virtual geomagnetic pole (VGP).

393 **Table DR5:** The published documents about magnetostratigraphy of PTB sections

Reference	Location	Section type	Host rock lithology	Age	Thickness / Number of samples	Zij. ?	RT	FT	BT	Correlation methods
(Gurevich and Slautsitays, 1985)	Novaya Zemlya, Russia	Terrestrial	sandstones	P3	1) Eastern limb: 1000 m / 460 samples 2) Western limb: 1200 m / 290 samples	×	/	/	/	the flora and marine fauna
(Heller et al., 1988)	Shangsi, China	Marine	limestones	P3-T1	130 m / 190 samples	√	×	/	/	/
(McFadden et al., 1988)	Tarim Basin, China	Terrestrial	conglomerates, sandstones	P-T	1) 870 m / 170 samples 2) 240 m / 64 samples	√	/	/	/	fossiliferous stratigraphy
(Li and Wang, 1989)	Meishan, China	Marine	limestones	P3-T1	~60 m / 111 samples	√	/	/	/	fossiliferous stratigraphy
(Steiner et al., 1989)	Shangsi, China	Marine	limestones	P3-T1	1) GPW: 198 m / 236 samples 2) LP: 112 m / 48 samples 3) HPT: 960 m / 217 samples	√	/	/	/	ammonites, conodonts, brachiopods
(Haag and Heller, 1991)	Nammal gorge, Pakinstan	Marine	limestones, domilite	P3	220 m / 220 samples	√	/	/	/	brachiopods, ammonites
(Gurevitch et al., 1995)	Western Taimyr, Russia	Siberian Trap	magic magmatism	248.2-251.2 Ma	>1500 m / 31 samples	√	A	√	/	geochronology
(Heller et al., 1995)	Sichuan, China	Marine	carbonate	P3-T1	1) Linshui: 300 m / 146 samples 2) Shuijiang: 70 m / 57 samples 3) Wulong: 300 m/ 216 samples	√	×	×	/	conodonts, ammonites, fusulina
(Embleton et al., 1996)	Taiyuan, North China	Terrestrial	red shales, red sandsotnes	P1-P3	1201 ~ 1300 m /286 samples	√	×	/	/	brachiopods, corals, fusilinids
(Gialanella et al., 1997)	Monastirskoje, Russian	Terrestrial	red beds	P2-P3	150 m / 300 samples	√	/	√	/	bivalves, ostracodes
(Nawrocki, 1997)	the CEB, Poland	Terrestrial	sandstones, salts, carbonates	P2-T1	1) 15 outcrops / 93 samples 2) 11 unoriented boreholes / 630 samples	√	B	/	/	spores and pollens, conodonts
(Besse et al., 1998)	Shahreza, Iran	Marine	limestones	P3-T1	~ 20 m / 80 samples	√	B	/	/	/
(Zhu and Liu, 1999)	Meishan, China	Marine	limestones	P3-T1	~ 60 m / 209 samples	×	/	/	/	fossiliferous stratigraphy
(Gallet et al., 2000)	Abadeh, Iran	Marine	limestones	P3-T1	? / 130 samples	√	B	/	/	conodont zones
(Meng et al., 2000)	Meishan, China	Marine	limestones	P3-T1	~60 m / 330 samples	×	/	/	/	fossiliferous stratigraphy
(Scholger et al., 2000)	Southern Alps, Italy	Marine	carbonates	P3-T1	1) Bulla section: 371 samples 2) Siusi section: ~560 samples	√	1) Bulla: B 2) Siusi: C	/	/	fusulinids, foraminifers, calcareous algae, brachiopods.
(Szurlies et al., 2003)	the CEB, Germany	Terrestrial	sandstones, salts, carbonates	P3-T1	eight outcrops and one completely cored well / ~900 samples	√	√	/	/	conchostracans, Gamma-ray logs
(De Kock and Kirschvink, 2004)	Karoo Basin, south Africa	Terrestrial	sandstones, mudstones	P3-T1	130 m / 63 samples	√	×	/	/	vertebrate fossils
(Gurevitch et al., 2004)	Noril'sk and Abagalakh	Siberian Trap	Basalts	249 ~251 Ma	~ / 400 samples	√	/	/	/	U-Pb ages
(Nawrocki, 2004)	the CEB, Poland	Terrestrial	red beds	P3-T1	~ / 27 samples	√	/	/	/	conchostracans
(Burov, 2005)	the Kichmenga River basin, Russia	Terrestrial	claystones	P3-T1	~15 m / 50 samples	×	/	/	/	vertebrate fossils
(Ward et al., 2005)	Karoo Basin, south Africa	Terrestrial	sandstones, mudstones	P3-T1	1) East Lootsberg Pass: ~130 m / ~ 2) West Lootsberg Pass: ~285 m / ~ 3) Komandodriftdam : ~135 m / ~	×	B	/	√	vertebrate fossils
(Szurlies, 2007)	the CEB, Germany	Terrestrial	red beds	P3 - T2	1.3 km (16 outcrops and 6 cores) / 2050 samples	√	/	√	/	gamma-ray logs, fossiliferous stratigraphy
(Glen et al., 2009)	Shangsi(S), Langdai(L) and the southern Junggar Basin(J), China	1) S: marine 2) L: terrestrail to shallow marine 3) J: terrestrail	1) S: carbonates 2) L: paralic mudstones and carbonates 3) J: sandstones	P3-T1	1) Si : 170 m / 286 samples in total 2) L : ~80 m /over 100 samples in total 3) J : ~350 m / over 300 samples in total	√	1) S: / 2) L: / 3) J: √	1) S: × 2) L: √ 3)J: /	/	biostratigraphy
(Iosifidi and Khramov, 2009)	Pai-Khoi, Russia	Terrestrial	sandstones	P3, possible	400 m / 100 samples	√	C	×	/	/
(Szurlies et al., 2012)	the CEB, Netherlands	Terrestrial	sandstones, siltstones and carbonates	P3-T1	100 m / 80 samples	√	×	/	/	conchostracan, gamma-ray logs, cyclostratigraphy
(Gastaldo et al., 2015)	Karoo Basin, south Africa	Terrestrial	sandstones, mudstones	P3-T1	~ / 123 samples	√	/	/	/	flora taxa, vertebrate fossils, U-Pb ages
(Scholze et al., 2017)	the CEB, Germany	Terrestrial	siliciclastics, limestones	P3-T1	65 m / 91 samples	√	/	/	/	isotope-chemostratigraphy, palynology, conchostracan biostratigraphy
(Gastaldo et al., 2018)	Karoo Basin, south Africa	Terrestrial	sandstones, mudstones	P3-T1	240 m / ~	√	/	/	/	flora taxa, vertebrate fossils, U-Pb ages, lithostratigraphy

Notes: RT = reversal test, FT= fold test, BT = baked contact test, PTB = Permian-Triassic boundary, the CEB = the Central European Basin, Zij.? = does the document provide stable demangetization results?.